Exploring Sources of Ice Crystals in Cirrus Clouds: Comparative Analysis of Two Ice Nucleation Schemes in CAM6

Kai Lyu[1], Xiaohong Liu[1], Bernd Kärcher[2]

[1]Department of Atmospheric Sciences, Texas A&M University, College Station, 77840, USA
[2]DLR Institut für Physik der Atmosphäre, Oberpfaffenhofen, Wessling, 82234, Germany

Correspondence to: Xiaohong Liu (xiaohong.liu@tamu.edu)

Abstract. Ice nucleation, a critical process in cirrus clouds, remains a challenge in global climate models. To enhance the understanding, a novel ice nucleation parameterization based on the Kärcher (2022) (K22) scheme is introduced into the NCAR Community Atmosphere Model version 6 (CAM6).

To investigate ice formation in cirrus clouds, sensitivity tests are conducted to analyze three ice sources from~~:~~ orographic gravity wave (OGWs)~~-induced~~, convecti~~veon~~ ~~detrained~~ detrainment, and turbulence~~-induced~~. These tests employ both the K22 scheme and the default Liu and Penner (2005) (LP05) scheme. Model evaluation includes 6-year climatology and nudged simulations representing the Small Particles in Cirrus (SPARTICUS) and O2/N2 Ratio and CO2 Airborne Southern Ocean Study (ORCAS) campaigns.

~~The climatology simulations reveal that both schemes~~Both schemes simulate that convection ~~concentrate~~ detrained and turbulence-induced ice crystals are concentrated in low- to mid-latitudes, whereas OGW-induced ice crystals are concentrated in mid- to high latitudes. Compared to the LP05 scheme, the K22 scheme generates a higher number of ice crystals. The simulated cloud microphysical properties using the K22 scheme align well with observations for orographic cirrus during the SPARTICUS campaign.

In orographic cirrus over high terrains at mid- to high latitudes, both schemes identify OGW-induced ice crystals as the dominant ice source. However, due to distinct competition parameterizations, the K22 scheme exhibits less competition from minor ice sources (convection detrained and turbulence-induced). This underscores the significance of competition mechanisms within nucleation schemes for accurate cirrus clouds simulation. The application of two distinct nucleation schemes provides valuable insights into the dominant ice sources in cirrus clouds.

Formatted: Indent: First line: 0 cm

Formatted: Indent: First line: 0 cm

1. Introduction

Cirrus clouds play an important role in the Earth's radiation budget, thereby affecting the climate (Liou, 1986). These ice clouds can reflect solar radiation back to space, cooling the planet (Chen et al., 2024; Forster et al., 2023)~~(Chen et al., 2024; Chen et al., 2000; "The Earth's Energy Budget, Climate Feedbacks and Climate Sensitivity," 2023; Forster et al., 2023)~~. They can also absorb terrestrial longwave radiation and thus warm the planet. The balance between these two opposite processes is greatly influenced by the microphysical properties of ice crystals in cirrus clouds and determines the net cloud radiative forcing. The representation of cirrus clouds in global climate models (GCMs) has been recognized as a key factor in understanding the climate change (Boucher et al., 2013).

Ice crystals in cirrus clouds originate from two main processes, detrainment from convective clouds and in-situ nucleation (Krämer et al., 2016; Muhlbauer, Ackerman, et al., 2014). Cirrus clouds are formed through convective detrainment when air containing ice crystals flows out of convective clouds, such as anvils. These clouds are usually associated with high ice number concentrations (> 100 L^{-1}) (Heymsfield et al., 2017).

Ice crystals in in-situ cirrus clouds, such as orographic cirrus over high terrains, are primarily nucleated by aerosols. There are two nucleation mechanisms: homogeneous freezing of solution droplets and heterogeneous nucleation on ice nucleating particles (INPs). Homogeneous nucleation requires higher supersaturation (> ~40-60 %) and lower temperatures (< -37 °C), typically resulting in high ice number concentrations (> 100 L^{-1}). In contrast, heterogeneous nucleation occurs at lower supersaturation and higher temperatures, involving INPs such as dust and black carbon (BC). This process generally produces low ice number concentrations (< 100 L^{-1}) (Froyd et al., 2022; Heymsfield et al., 2017).

Substantial progress has been made in understanding homogeneous nucleation (Koop et al., 2000). Homogeneous nucleation is usually triggered by high vertical velocities (> 0.1 m s^{-1}). These dynamic factors can be induced by either turbulence in the unstable circumstances with small Richardson numbers or gravity waves in the stable atmosphere with large Richarson numbers (Heymsfield et al., 2017).

Recent studies on cirrus clouds in GCMs usually overlook the roles of ice crystal sources, especially for cirrus clouds with high ice number concentrations (> 100 L^{-1}). The absence or misrepresentation of a critical ice source may lead to the failure to simulate cirrus cloud properties. For example, most GCMs treat turbulence as the sole subgrid-scale vertical

velocity mechanism driving ice nucleation. However, research has shown that due to limitations in higher-order turbulence closure theory, cirrus clouds formed by gravity waves are usually absent in GCMs (Golaz et al., 2002b; Huang et al., 2020). Notably, studies have demonstrated that incorporating the effects of orographic gravity waves (OGWs) into ice nucleation processes enables models to successfully simulate the observed characteristics of orographic cirrus clouds (Lyu et al., 2023). In addition, many studies highlight that ice crystals from convective detrainment can have a significant impact on the microphysical properties of cirrus clouds, particularly in the tropical regions (Horner & Gryspeerdt, 2023; Horner & Gryspeerdt, 2024; Nugent et al., 2022). In this study, we focus on three ice sources: OGW-induced, turbulence-induced and convective detrained.

~~Significant uncertainties persist regarding heterogeneous nucleation (Hoose & Möhler, 2012; Murray et al., 2012) and the interplay between the two nucleation mechanisms (Kärcher et al., 2022; Shi et al., 2015). There are many uncertainties in the nucleation processes and can complicate the prediction of cirrus clouds microphysical properties (Knopf & Alpert, 2023).~~ Aerosols such as dust, soot, metallic particles, and biological particles, can act as INPs, inducing heterogeneous nucleation and potentially suppressing homogeneous nucleation (Fan et al., 2016; Froyd et al., 2022; Heymsfield et al., 2017; Kärcher & Ström, 2003; Knopf & Alpert, 2023). The activation efficiency of INPs is determined by their chemical components, which is highly dependent on their sources (Beall et al., 2022; Chen et al., 2024; Tobo et al., 2019).

~~Moreover, uncertainties regarding~~Limited knowledge of the number concentration, ~~and~~ chemical composition, and activation efficiency of INPs in the upper troposphere complicates the model prediction of cirrus clouds microphysical properties (Kärcher et al., 2022; Knopf & Alpert, 2023)~~along with their nucleation mechanisms further hinder cirrus cloud simulations (DeMott et al., 2011)~~. Moreover, currently conventional GCMs cannot resolve the subgrid-scale vertical velocity, which drives the water vapor supersaturation for ice nucleation, posing additional uncertainty for model simulations. ~~(Ullrich et al., 2017)~~

Several parameterizations of nucleation mechanisms have been developed in GCMs. Liu and Penner (2005) (LP05) developed a parameterization that includes homogeneous nucleation, heterogeneous nucleation and their interactions. The parameterization was subsequently applied to the NCAR Community Atmospheric Model (CAM) (Liu et al., 2007) and was further refined to include the effects of pre-existing ice (Shi et al., 2015).

A new parameterization (Kärcher, 2022), referred to as K22, that encompasses homogeneous nucleation, heterogeneous nucleation, their interactions, and competition with preexisting cirrus ice, has been integrated into CAM6. The purpose of this paper is to integrate the K22 nucleation parameterization into GCMs and evaluate its effects on cloud microphysical properties and dominant sources of ice crystals in cirrus clouds. Section 2 presents a description of the model, and the parameterization method used in the study. The observational data employed for evaluation are described in Section 3. The model results, along with comparisons to the default LP05 parameterization, are discussed in Section 4. Finally, the summary and conclusions are presented in Section 5.

2. Model and Parameterization

2.1 Model Description

~~2.1~~ The NCAR Community Atmosphere Model version 6 (CAM6) model is the atmosphere component of Community Earth System Model version 2 (CESM2) (Danabasoglu et al., 2020). CAM6 employs the updated Morrison-Gettelman cloud microphysics scheme (MG2) to predict the mass and number concentrations of cloud liquid, cloud ice, rain and snow (Gettelman & Morrison, 2015; Morrison & Gettelman, 2008). The deep convection processes are represented using the Zhang and McFarlane (1995) scheme. The planetary boundary layer turbulence, cloud macrophysics, and shallow convection are treated by the Cloud Layers Unified by Bi-normals (CLUBB) (Bogenschutz et al., 2013; Golaz et al., 2002a; Hinz et al., 1996). Aerosols are treated using the 4-mode version of Modal Aerosol Model (MAM4) (Liu et al., 2016). Since CLUBB effectively represents turbulence with a small Richardson number but struggles to produce perturbations caused by gravity waves (Golaz et al., 2002a, 2002b; Huang et al., 2020), subgrid-scale vertical velocities from orographic gravity waves (OGWs) and turbulence are incorporated into the ice nucleation schemes (Lyu et al., 2023). The turbulence-driven vertical velocity is derived from turbulence kinetic energy (TKE) calculated by CLUBB. Aerosols involved in ice nucleation act interactively with the MAM4. When new ice crystals form, the nucleated aerosols are transferred from the interstitial state to the cloud-borne state. Similarly, when cloud droplets form, the nucleated aerosols are transferred to the cloud-borne state and are subject to precipitation scavenging. The radiation calculations are based on the Rapid Radiative Transfer Model for General Circulation Models (RRTMG) (Iacono et al., 2008).

Formatted: Normal, Indent: First line: 0.63 cm, Line spacing: Double, No bullets or numbering

Formatted: Font: (Asian) +Body Asian (宋体), (Asian) Chinese (Simplified, Mainland China)

The NCAR Community Atmosphere Model version 6 (CAM6) model is the atmosphere component of Community Earth System Model version 2 (CESM2) (Danabasoglu et al., 2020). CAM6 employs the updated Morrison-Gettelman cloud microphysics scheme (MG2) to predict the mass and number concentrations of cloud liquid, cloud ice, rain and snow (Gettelman & Morrison, 2015; Morrison & Gettelman, 2008). The deep convection processes are represented using the Zhang and McFarlane (1995) scheme. The planetary boundary layer turbulence, cloud macrophysics, and shallow convection are treated by the Cloud Layers Unified by Bi-normals (CLUBB) (Bogenschutz et al., 2013; Golaz et al., 2002a; Hinz et al., 1996). Aerosols are treated using the 4-mode version of Modal Aerosol Model (MAM4) (Liu et al., 2016). Since CLUBB effectively represents turbulence with a small Richardson number but struggles to produce perturbations caused by gravity waves (Golaz et al., 2002a, 2002b; Huang et al., 2020), subgrid-scale orographic gravity waves (OGWs) and turbulence kinetic energy (TKE) from CLUBB (CLUBB-TKE) are introduced into the ice nucleation as sources of vertical velocity (Lyu et al., 2023). Aerosols involved in ice nucleation act interactively with the MAM4. When new ice crystals form, the nucleated aerosols are transferred from the interstitial state to the cloud-borne state. Similarly, when cloud droplets form, the nucleated aerosols are transferred to the cloud-borne state and are subject to precipitation scavenging. The radiation calculations are based on the Rapid Radiative Transfer Model for General Circulation Models (RRTMG) (Iacono et al., 2008). The climatology experiments and nudged simulations related to the Small Particles in Cirrus (SPARTICUS) and O2/N2 Ratio and CO2 Airborne Southern Ocean Study (ORCAS) campaigns are designed and listed in Table 1 and 2. All simulations are conducted at a resolution of 0.9º × 1.25º with 56 vertical layers.

The LP05 ice nucleation scheme involves two mechanisms: homogeneous and heterogeneous nucleation (Liu & Penner, 2005). Developed base on numerical parcel model simulations, this scheme considers the competition between homogeneous and heterogeneous nucleation processes, as well as their interactions with pre-existing ice crystals (Shi et al., 2015). Koop et al. (2000)To fit to observed ice number concentrations (Gettelman et al., 2010), homogeneous nucleation utilizes sulfate aerosols in the Aitken mode with diameters greater than 0.1 μm.

In our study, the OGW experiments serve as the reference experiments. These experiments consider three primary sources of ice crystals: convective detrainment, nucleation driven by turbulence (CLUBB-TKE), and nucleation driven by OGWs. To isolate the effects of each source, we designed three sensitivity tests: no_DET, no_TKE and no_OGW, each

excluding one of these specific sources. By comparing the differences in ice number concentration (N_i) between the reference experiments and sensitivity experiments, we can aim to understand the contribution of each ice source in CAM6.

Table 1 Description of 6-year Climatology Simulations

Model experiment	*Description*
LP05_OGW-Climo	Default CAM6 configuration with turbulence (CLUBB-TKE) and orographic gravity waves (OGWs) for ice nucleation.
LP05_no_OGW-Climo	Same as LP05_OGW-Climo but without OGWs for ice nucleation
LP05_no_DET-Climo	Same as LP05_OGW-Climo but without detrained ice.
LP05_no_TKE-Climo	Same as LP05_OGW-Climo but without turbulence for ice nucleation.
LP05_OGW-Homo-Climo	Same as LP05_OGW-Climo but only consider homogeneous ice nucleation.
LP05_OGW-Hete-Climo	Same as LP05_OGW-Climo but only consider heterogenous ice nucleation.
K22_OGW-Climo	Same as LP05_OGW-Climo but with K22 nucleation parameterization.
K22_no_OGW-Climo	Same as LP05_no_OGW-Climo but with K22 nucleation parameterization.
K22_no_DET-Climo	Same as LP05_no_DET-Climo but with K22 nucleation parameterization.
K22_no_TKE-Climo	Same as LP05_no_TKE-Climo but with K22 nucleation parameterization.
K22_OGW-Homo-Climo	Same as K22_OGW-Climo but only consider homogeneous ice nucleation.
K22_OGW-Hete-Climo	Same as K22_OGW-Climo but only consider heterogenous ice nucleation.
K22_OGW_Shan-Climo	Same as K22_OGW-Climo but with aerosol wet removal in convection (Shan et al., 2021).

Formatted: Normal, Indent: First line: 0.63 cm, Line spacing: Double, Don't keep with next

Formatted: Indent: First line: 0.63 cm, Space After: 0 pt, Line spacing: Double

Formatted: Indent: First line: 0.63 cm, Line spacing:

Formatted: Indent: First line: 0.63 cm, Line spacing:

Formatted: Indent: First line: 0.63 cm, Line spacing:

Formatted: Indent: First line: 0.63 cm, Line spacing:

Formatted: Indent: First line: 0.63 cm, Line spacing:

Formatted: Indent: First line: 0.63 cm, Line spacing:

Formatted: Indent: First line: 0.63 cm, Line spacing:

Formatted: Indent: First line: 0.63 cm, Line spacing:

Formatted: Indent: First line: 0.63 cm, Line spacing:

Formatted: Indent: First line: 0.63 cm, Line spacing:

Formatted: Indent: First line: 0.63 cm, Line spacing:

Formatted: Indent: First line: 0.63 cm, Line spacing:

130

Formatted: Normal, Indent: First line: 0.63 cm, Line spacing: Double, Don't keep with next

Table 2 Description of Nudged Simulations

Model experiment	*Description*
2009 October to 2010 June	
LP05_OGW-SP	Default CAM6 configuration with turbulence and orographic gravity waves (OGWs) for ice nucleation.
LP05_no_OGW-SP	Same as LP05_OGW-SP but without OGWs for ice nucleation
LP05_no_DET-SP	Same as LP05_OGW-SP but without detrained ice.
LP05_no_TKE-SP	Same as LP05_OGW-SP but without turbulence for ice nucleation.
K22_OGW-SP	Same as LP05_OGW-SP but with K22 nucleation parameterization.
K22_no_OGW-SP	Same as LP05_no_OGW-SP but with K22 nucleation parameterization.
K22_no_DET-SP	Same as LP05_no_DET-SP but with K22 nucleation parameterization.
K22_no_TKE-SP	Same as LP05_no_TKE-SP but with K22 nucleation parameterization.
K22_OGW-Homo-SP	Same as K22_OGW-SP but only consider homogeneous ice nucleation.
K22_OGW-Hete-SP	Same as K22_OGW-SP but only consider heterogenous ice nucleation.
2015 October to 2016 February	
LP05_OGW-OR	Same as LP05_OGW-SP except simulation period.
LP05_no_OGW-OR	Same as LP05_no_OGW-SP except simulation period.
LP05_no_DET-OR	Same as LP05_no_DET-SP except simulation period.
LP05_no_TKE-OR	Same as LP05_no_TKE-SP except simulation period.
K22_OGW-OR	Same as K22_OGW-SP except simulation period.
K22_no_OGW-OR	Same as K22_no_OGW-SP except simulation period.
K22_no_DET-OR	Same as K22_no_DET-SP except simulation period.
K22_no_TKE-OR	Same as K22_no_TKE-SP except simulation period.

Formatted: Indent: First line: 0.63 cm, Line spacing:

Formatted: Normal, Indent: First line: 0.63 cm, Line spacing: Double, Don't keep with next

Formatted: Indent: First line: 0.63 cm, Space After: 0 pt, Line spacing: Double

Formatted: Indent: First line: 0.63 cm, Space After: 0 pt, Line spacing: Double

Formatted: Indent: First line: 0.63 cm, Line spacing:

Formatted: Indent: First line: 0.63 cm, Line spacing:

Formatted: Indent: First line: 0.63 cm, Line spacing:

Formatted: Indent: First line: 0.63 cm, Space After: 0 pt, Line spacing: Double

Formatted: Indent: First line: 0.63 cm, Line spacing:

Formatted: Indent: First line: 0.63 cm, Line spacing:

Formatted: Indent: First line: 0.63 cm, Line spacing:

Formatted: Indent: First line: 0.63 cm, Line spacing:

Formatted: Indent: First line: 0.63 cm, Line spacing:

Formatted: Indent: First line: 0.63 cm, Line spacing:

Formatted: Indent: First line: 0.63 cm, Line spacing:

Formatted: Indent: First line: 0.63 cm, Line spacing:

Formatted: Indent: First line: 0.63 cm, Line spacing:

Formatted: Indent: First line: 0.63 cm, Line spacing:

Formatted: Indent: First line: 0.63 cm, Line spacing:

Formatted: Indent: First line: 0.63 cm, Line spacing:

Formatted: Indent: First line: 0.63 cm, Line spacing:

2.2 ~~K22~~ Ice Nucleation Parameterizations

2.2.1 K22 Scheme

In the K22 parameterization, ~~,~~ homogeneous freezing is treated as a stochastic process in which the number of activated solution droplets ~~decreases~~ (n_{homo}) over time based on freezing rate (j) ($n_{homo} = \int j dt$). The freezing rate is determined using the liquid water volume (V) of the droplet population and a rate coefficient (J) derived from a water activity-based formula (Koop et al., 2000) ($j = VJ$). Vertical velocity (w), supersaturation with respect to ice (S_i), and temperature (T) significantly influence~~s~~ water activity ($J = J(w, S_i, T)$) (Baumgartner et al., 2022; Kärcher et al., 2022; Liu & Penner, 2005). The scheme assumes a monodisperse liquid solution droplet distribution at a wet radius of 0.25 μm. The formulation of the number of ice crystals nucleated homogeneously is described by Kärcher et al. (2022).

For heterogeneous nucleation, a~~A~~ deterministic (time-independent) approach to predict the number (n) of activated INPs is employed in the K22 parameterization as follows:

$$n = n_{tot}\Phi(s), \tag{1}$$

where n_{tot} is the number concentration of INPs (e.g., coarse mode dust) ~~the total INP number concentration~~ and Φ is the activated INP fraction. Φ can be represented as either a linear ramp or a hyperbolic tangent function. Since we consider dust as the INPs, a linear ramp is applied in our study.

The function Φ can be expressed as follows:

$$\Phi = \begin{cases} 0 & : \ s < s_{min} \\ \frac{(s - s_{min})}{s_{max} - s_{min}} & : s_{min} \le s \le s_{max}, \\ 1 & : \ s > s_{max} \end{cases} \tag{2}$$

where s_{min} and s_{max} are two parameters that define the range of ice supersaturation where heterogeneous nucleation can occur. In our study, they are set to 0.22 and 0.3, respectively.

The equation governing the temporal evolution of ice supersaturation, s, in the ice-vapor system is expressed as

$$\frac{ds}{dt} = a(s+1)w - \int_0^s \frac{4\pi}{v n_{sat}} \frac{dn}{ds'} \left(\int_{\tau(s')}^{t(s)} r^2 \frac{dr}{dt} dt \right) ds' , \tag{3}$$

Formatted: Indent: First line: 0.63 cm

Formatted: Font: Italic
Formatted: Subscript
Formatted: Font: Italic
Formatted: Font: Italic
Formatted: Font: Italic
Formatted: Font: Italic
Formatted: Font: Italic
Formatted: Font: Italic
Formatted: Subscript
Formatted: Font: Italic
Formatted: Font: Italic
Formatted: Font: Italic
Formatted: Font: Italic
Formatted: Font: Italic

where $\frac{ds}{dt}$ represents the time derivative of s. The first term on the right-hand side of the equation is the production term related to adiabatic cooling. a is a ~~thermaldynamic~~ thermodynamic parameter (Pruppacher et al., 1998) relating to adiabatic vertical air motion, and w is restricted to the updraft speed ($w > 0$). The second term signifies the loss term due to the removal of water vapor. The upper integration limit is the time t corresponding to ice supersaturation s, and the lower integration limit is a time τ corresponds to $0 \leq s' \leq s$.

Within the integral, r is the radius of spherical ice crystals, $\frac{dr}{dt}$ denotes the associated growth rate per ice crystal, v represents the volume of one water molecule in bulk ice, and n_{sat} is the water vapor number concentration in gas phase at ice saturation. The number concentration of ice crystals formed by INPs in a range of supersaturation ds' is given by $\frac{dn}{ds'}$.

The loss term in Equation (3) can be integrated numerically as described by Kärcher (2022). When $\frac{ds}{dt} = 0$, we can estimate the total heterogeneously nucleated ice number concentrations. Quenching velocities w_q are defined as:

$$w_q = \frac{\text{~~Loss term in Equation (3)~~} \int_0^s \frac{4\pi}{v n_{sat}} \frac{dn}{ds'} \left(\int_{\tau(s')}^{t(s)} r^2 \frac{dr}{dt} dt \right) ds'}{a(s+1)} , \quad (4)$$

where the loss term includes contributions from heterogeneous nucleation and pre-existing ice. This approach allows us to determine an effective vertical updraft w_{eff} which is used to describe conditions relevant to the homogeneous nucleation.

The effective vertical updraft speed w_{eff} is calculated as:

$$w_{eff} = w - w_{q,het} - w_{q,pre}, \quad (5)$$

where w is the updraft speed, $w_{q,\,het}$ is the quenching velocity for ice crystals due to heterogeneous nucleation, and $w_{q,pre}$ is the quenching velocity due to pre-existing ice. If $w_{eff} \leq 0$, no homogeneous freezing occurs. When $w_{eff} > 0$, homogeneous nucleation will take place, but homogeneously nucleating ice number concentration will be smaller than that in the absence of INP-derived and pre-existing ice crystals (i.e. that calculated based on w) ($n_{homo} = n_{homo}(w_{eff})$).

2.2.2 LP05 Scheme

The LP05 ice nucleation scheme incorporates two primary mechanisms: homogeneous and heterogeneous nucleation (Liu & Penner, 2005). It is based on fitted simulation results from a cloud parcel model with varying vertical velocities. The

Formatted: Font: Italic
Formatted: Subscript
Formatted: Font: Italic
Formatted: Subscript

maximum supersaturation is determined in the parcel model from the balance between the production due to adiabatic cooling by updrafts and loss due to vapor deposition on ice crystals. The number of nucleated ice crystals is derived based on ice supersaturation, temperature, aerosol number concentrations and composition, and vertical velocity. Subgrid-scale vertical velocity can be derived from TKE calculated by CLUBB, from OGWs, or from the combined contribution of both components.

Homogeneous nucleation in the LP05 scheme, similar to the K22 scheme, adopts the parameterizations by Koop et al. (2000). Sulfate aerosols in the Aitken mode with diameters greater than 0.1 μm is applied to fit to ice number concentrations (Gettelman et al., 2010). On the other hand, heterogeneous nucleation considers the coarse mode dust as potential source of INPs. The number of ice crystals formed due to heterogeneous nucleation n in the LP05 scheme is calculated using $n = n_{dust} \cdot \Phi(T, w, S_i)$, where n_{dust} is the coarse mode dust number concentration from MAM4, and Φ is active aerosol fraction, empirically derived as a function of temperature (T), vertical velocity (w), and ice supersaturation (S_i).

The LP05 scheme considers the competition between homogeneous and heterogeneous nucleation. It ~~(Kärcher et al., 2006)~~determines the critical dust INP concentration, above which homogeneous nucleation is completely switched off. Below that homogeneous nucleation occurs partially and is gradually transitioned to the pure homogeneous nucleation at lower INP concentrations. The LP05 scheme is modified to consider the effect of pre-existing ice crystals (Shi et al., 2015), which is parameterized by reducing the vertical velocity for ice nucleation as a result of water vapor deposition on pre-existing ice~~(Kärcher et al., 2006)~~.

2.2.3 Differences Between Two Schemes

The K22 scheme incorporates a physically-based competition of various ice sources grounded in a quasi-kinetic nucleation framework. It simulates the simultaneous evolution of both homogeneous and heterogeneous nucleation rates in response to changing supersaturation and aerosol properties. The framework allows a flexible parameterization of activation efficiencies of different INPs types. This approach explicitly tracks the kinetic interplay between pre-existing ice and different ice formation pathways, allowing for transient coexistence and interaction.

The LP05 scheme addresses the competition between nucleation mechanisms and pre-existing ice through an empirical framework derived from parcel model simulations. In this framework, supersaturation is implicitly partitioned, with the

nucleation pathway most favorable under the given conditions being prioritized. Heterogeneous nucleation is favored at lower supersaturations and higher dust concentrations, while homogeneous nucleation predominates at higher supersaturations and lower dust concentrations. Pre-existing ice crystals are typically used as a threshold to judge whether new ice can be formed.

~~There are some differences in the competition with pre-existing ice between the K22 and LP05 nucleation schemes.~~ Overall, the K22 scheme provides a more continuous and interactive treatment of multiple ice nucleation pathways, with a stronger emphasis on the dynamic interplay between supersaturation, aerosol concentrations, and pre-existing ice crystals. On the other hand, the LP05 scheme employs a stepwise approach that directly compares the potential for nucleation with the concentration of pre-existing ice crystals, imposing a threshold when nucleation occurs. Uncertainties exist regarding the relationship between the reduction of supersaturation and the suppression of nucleation caused by pre-existing ice crystals ~~and the number of homogeneously nucleated ice crystals suppressed by pre-existing ice crystals~~. This relationship and its impact on the number of nucleated ice crystals requires further investigation.

The different strategies for representing ice nucleation pathways lead to stronger suppression of new ice formation in the LP05 scheme compared to the K22 scheme. In the LP05 scheme, competition between nucleation pathways is handled sequentially. Heterogeneous nucleation occurs first, followed by homogeneous nucleation only if the supersaturation exceeds a threshold (Liu & Penner, 2005). In addition, pre-existing ice crystals consume supersaturation before any new nucleation can occur (Kärcher et al., 2006; Shi et al., 2015), which further suppress new ice formation. In contrast, the K22 scheme represents homogeneous nucleation, heterogeneous nucleation, and pre-existing ice growth within a unified framework, allowing all processes to occur simultaneously.~~(Kärcher et al., 2006; Shi et al., 2015)~~ As a result, for example, when the number concentration of pre-existing ice crystals is high, the LP05 scheme strongly suppresses new ice formation due to its sequential competition approach. Meanwhile, the K22 scheme permits new ice formation by accounting for concurrent interactions among all ice-related processes, even under conditions where the LP05 scheme would inhibit nucleation.~~In the K22 parameterization quenching velocity, which is determined using a loss term associated with pre-existing ice crystals, is employed to calculate the number of homogeneously nucleated ice crystals.~~

~~However, the LP05 parameterization estimates the homogeneously nucleated ice number from a different perspective. The scheme first assumes the absence of pre-existing ice crystals and calculates the ice number that would be generated homogeneously. The calculated ice number is then compared the pre-existing ice number. If the pre-existing ice number is smaller than the calculated number, additional ice crystals are generated homogeneously, with the resulting ice crystal count equal to the difference. Otherwise, no new ice crystals are nucleated.~~In the K22 parameterization quenching velocity, which is determined using a loss term associated with pre-existing ice crystals, is employed to calculate the number of ~~homogeneously nucleated ice crystals.~~

~~Since the K22 scheme assumes spherical ice crystal shapes, it may underestimate the surface area available for vapor deposition. This underestimation can exaggerate when pre-existing ice crystals are small and numerous. This bias may lead to an underestimation of supersaturation depletion by these ice crystals, potentially facilitating the occurrence of homogeneous nucleation. However, the LP05 scheme emphasizes competition between newly nucleated and pre-existing ice crystals, influenced by the large size of model grid. If a small fraction of the grid contains high concentrations of pre-existing ice crystals, the LP05 scheme can suppress new ice formation even when new clouds form elsewhere within the same grid.~~

2.3 Experiment Descriptions

Formatted: Heading 2, Indent: Left: 0 cm, Hanging: 0.63 cm, Line spacing: single, Outline numbered + Level: 2 + Numbering Style: 1, 2, 3, … + Start at: 1 + Alignment: Left + Aligned at: 0.63 cm + Indent at: 1.27 cm

The climatology experiments and nudged simulations related to the Small Particles in Cirrus (SPARTICUS) and O2/N2 Ratio and CO2 Airborne Southern Ocean Study (ORCAS) campaigns are designed and listed in Table 1 and 2. All simulations are conducted at a resolution of 0.9º × 1.25º with 56 vertical layers. We focus on the SPARTICUS and ORCAS campaigns in this study because they provide critical data on OGW-induced ice crystals. The SPARTICUS campaign involves flights over the mountainous regions from winter to summer, while the ORCAS campaign focuses on both ocean and continental regions during the summer.

In this study, the OGW experiments serve as the reference experiments. These experiments consider three primary sources of ice crystals: convective detrainment, nucleation driven by turbulence (CLUBB-TKE), and nucleation driven by OGWs. To isolate the effects of each source, we designed three sensitivity experiments: no_DET (no detrainment), no_TKE (no CLUBB-TKE) and no_OGW (no OGWs), each excluding one of these specific sources. By comparing the differences in

ice number concentration (N_i) between the reference experiments and sensitivity experiments, we aim to understand the contribution of each ice source in CAM6.

Table 1 Description of 6-year Climatology Simulations

Model experiment	*Description*
LP05_OGW-Climo	Default CAM6 configuration with turbulence (CLUBB-TKE) and orographic gravity waves (OGWs) for ice nucleation.
LP05_no_OGW-Climo	Same as LP05_OGW-Climo but without OGWs for ice nucleation
LP05_no_DET-Climo	Same as LP05_OGW-Climo but without detrained ice.
LP05_no_TKE-Climo	Same as LP05_OGW-Climo but without turbulence for ice nucleation.
LP05_OGW-Homo-Climo	Same as LP05_OGW-Climo but only consider homogeneous ice nucleation.
LP05_OGW-Hete-Climo	Same as LP05_OGW-Climo but only consider heterogenous ice nucleation.
K22_OGW-Climo	Same as LP05_OGW-Climo but with K22 nucleation parameterization.
K22_no_OGW-Climo	Same as LP05_no_OGW-Climo but with K22 nucleation parameterization.
K22_no_DET-Climo	Same as LP05_no_DET-Climo but with K22 nucleation parameterization.
K22_no_TKE-Climo	Same as LP05_no_TKE-Climo but with K22 nucleation parameterization.
K22_OGW-Homo-Climo	Same as K22_OGW-Climo but only consider homogeneous ice nucleation.
K22_OGW-Hete-Climo	Same as K22_OGW-Climo but only consider heterogenous ice nucleation.
K22_OGW_Shan-Climo	Same as K22_OGW-Climo but with aerosol wet removal in convection (Shan et al., 2021).

Table 2 Description of Nudged Simulations

Model experiment	*Description*
2009 October to 2010 June	
LP05_OGW-SP	Default CAM6 configuration with turbulence and orographic gravity waves (OGWs) for ice nucleation.
LP05_no_OGW-SP	Same as LP05_OGW-SP but without OGWs for ice nucleation
LP05_no_DET-SP	Same as LP05_OGW-SP but without detrained ice.
LP05_no_TKE-SP	Same as LP05_OGW-SP but without turbulence for ice nucleation.
K22_OGW-SP	Same as LP05_OGW-SP but with K22 nucleation parameterization.
K22_no_OGW-SP	Same as LP05_no_OGW-SP but with K22 nucleation parameterization.
K22_no_DET-SP	Same as LP05_no_DET-SP but with K22 nucleation parameterization.
K22_no_TKE-SP	Same as LP05_no_TKE-SP but with K22 nucleation parameterization.
K22_OGW-Homo-SP	Same as K22_OGW-SP but only consider homogeneous ice nucleation.
K22_OGW-Hete-SP	Same as K22_OGW-SP but only consider heterogenous ice nucleation.
2015 October to 2016 February	
LP05_OGW-OR	Same as LP05_OGW-SP except simulation period.
LP05_no_OGW-OR	Same as LP05_no_OGW-SP except simulation period.
LP05_no_DET-OR	Same as LP05_no_DET-SP except simulation period.
LP05_no_TKE-OR	Same as LP05_no_TKE-SP except simulation period.
K22_OGW-OR	Same as K22_OGW-SP except simulation period.
K22_no_OGW-OR	Same as K22_no_OGW-SP except simulation period.
K22_no_DET-OR	Same as K22_no_DET-SP except simulation period.
K22_no_TKE-OR	Same as K22_no_TKE-SP except simulation period.

Formatted: Font: (Default) +Headings (Times New Roman)

Formatted: Indent: First line: 0 cm

3. Observational Data

3.1 SPARTICUS campaign

This study utilizes observational data obtained during the SPARTICUS field campaign, conducted from January to June 2010 in the Central United States. The flight tracks of the campaign are depicted in Fig. 1a, covering approximately 150

research flight hours targeting cirrus clouds. Temperature measurements were conducted using the Rosemount probe Model 102 probe with a precision of ±0.5 ℃. Vertical velocity was measured by the Aircraft-Integrated Meteorological Measurement System-20 (AIMMS-20) instrument mounted on a Learjet 25 (Muhlbauer, Kalesse, et al., 2014). Ice crystals ~~in the~~with diameters ~~size~~ rangin~~g~~e ~~of~~from 10– to 3000 µm were measured using two-dimensional stereo-imaging probes (2D-S). The 2D-S probe minimizes biases in the number concentration of small-sized ice crystals by addressing ice shattering effects (Lawson, 2011). Observational data were sampled at a frequency of 1 Hz. A total of 6236 data samples are available in both observational and simulated datasets during the five days identified as orographic cirrus events (Muhlbauer, Ackerman, et al., 2014).

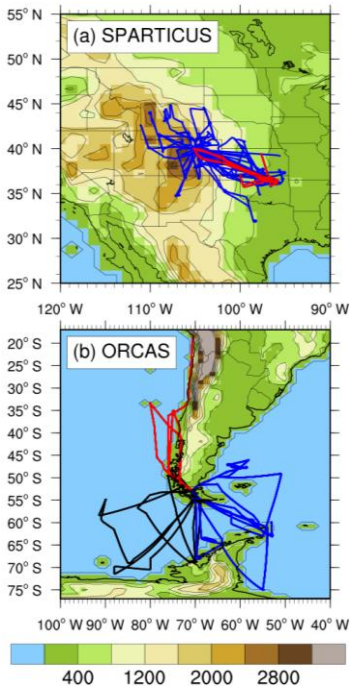

Figure 1. The top panel (a) shows aircraft trajectories (solid blue lines) during the SPARTICUS campaign. Solid red lines indicate flight tracks on days when orographic cirrus was observed (March 19, 30, April 1, 28, and 29, 2010). The bottom panel (b) shows aircraft trajectories during the ORCAS campaign. Color shading and black line contours illustrate the surface terrain (in m). Red lines denote flight tracks in Region 1, located north of Punta Arenas, Chile (SCCI), on the following days: January 23, and 25, February 8, 10, 17, 19, 22, 23 and 29, 2016. Blue lines denote flight tracks in Region 2, southeast of SCCI, on January 18, 25, and 30, February 12, 18, and 25, 2016. Black lines show flight tracks in Region 3, southwest of SCCI, on January 15, and 21, February 5 and 24, 2016.

At a speed of approximately 230 m s^{-1}, the aircraft covers about 100 km in 430 seconds of flight time, which corresponds to the model's horizontal resolution (1 degree). To facilitate a meaningful comparison between observational data and model outputs, a running average of 430 seconds of measurement data is applied (Patnaude et al., 2021). Additionally, the microphysical properties (such as ice number N_i, ice water content IWC and number-weighted diameters

D_{num}) of ice crystals with diameters larger than ~~10~~ 20 μm from CAM6 results are derived using the size cut method described by Eidhammer et al. (2014), consistent with the measurements obtained by the 2D-Stereo Particle Probe (2D-S) but excluding the first size bin. Recent study suggests excluding the 2D-S probe's first size bin (5-15 μm) to avoid overestimating ice number concentration (Jensen et al., 2013; Mitchell et al., 2024). We adopt the midpoint of the second size bin (15 - 25 μm), i.e., 20 μm, as the size threshold (Lyu et al., 2023) because hydrometeors smaller than 25 μm cannot be fully recorded (Glienke & Mei, 2019). However, disregarding measurements for particles smaller than 20 μm may overlook certain signatures of homogeneous freezing. To address this, we also provide supplementary results that include ice crystals with diameters larger than 10 μm, offering a more comprehensive analysis.

3.2 ORCAS campaign

The O_2/N_2 Ratio and CO_2 Airborne Southern Ocean Study (ORCAS) was an NSF-sponsored airborne field campaign conducted from Chile during January and February 2016. The campaign utilized the NSF/NCAR HIAPER Gulfstream V (GV) aircraft for 18 flights over a period of 6 weeks. The data, sampled at 1 Hz, encompasses a total of 95 flight hours (Stephens et al., 2018). Ice cloud particles are measured by the Fast 2-Dimensional Optical Array Cloud probe (Fast-2DC), which detects particle sizes ranging from 62.5 to 1600 μm (excluding the first two bins due to the ice shattering effects). The primary difference in measuring ice properties between the SPARTICUS and ORCAS campaigns is the instrumentation used to measure ice crystals. The SPARTICUS campaign employs the Fast 2D-S probe, while the ORCAS campaign utilizes the 2D-C probe. Due to the ice shattering effect, the reliability of small ice measurements is compromised with the 2D-C probe. The subsequent paragraphs will delve into ice microphysical properties, specifically focusing on large-size ice crystals (D_{num} ≥ 62.5μm) observed during the ORCAS campaign.

The ORCAS flight profiles encountered a lot of samples of cold upper-tropospheric clouds. To derive the properties (such as N_i, IWC and D_{num}) of ice crystals with diameter ≥ 62.5 μm from CAM6 results, the size cut method described by Eidhammer et al. (2014) is employed. This methodology ensures consistency with the measurements obtained by the 2D-C probe (Section 3.1).

To better evaluate the model results, this study divides the ORCAS flights into three regions, as illustrated in Fig. 1b. Flights in Region 1 primarily traverse high mountain ranges where cirrus clouds form primarily due to OGWs, together with

convection and frontal waves. Flights spanning Regions 2 and 3 predominantly cover oceanic areas, heavily influenced by convection and frontal waves. Notably, Region 2 is located downwind of the Andes Mountains and Antarctic high plateaus, thereby experiencing the additional influence from OGWs on observed cirrus cloud microphysical properties, while cirrus in Region 3 are less affected by OGWs.

This regional division allows for a more detailed analysis of cirrus cloud processes. The observed differences in cloud microphysical properties across these three regions highlight the distinct characteristics of cirrus clouds over land and ocean, particularly in mid- and high latitudes. These differences can provide insights into how various ice nucleation processes and environmental factors influence cirrus clouds formation and evolution.

4. Results

4.1 Climatology Experiments

Fig.2 illustrates the grid-mean ice number concentration (N_i) for different types of cirrus in climatology experiments using the LP05 and K22 schemes. The results indicate that N_i is generally higher in the K22_OGW-Climo experiment compared to the LP05_OGW-Climo experiment. In both schemes, ice crystals detrained from convection are primarily concentrated in the tropical regions and mid-latitudes, and in situ nucleated ice crystals induced by turbulence are prevalent near the tropical tropopause layers (TTL) and in mid-latitudes. In contrast, due to the presence of mountains and high plateaus, Oorographic cirrus due to OGWs are concentrated over mid- and high- latitudes, and in situ nucleated ice crystals induced by turbulence are prevalent at the top of tropical tropopause layers (TTL) and in mid-latitudes. Across all three ice sources, experiments based on the K22 scheme produce higher ice number concentrations than those based on the LP05 scheme, mainly from the OGW-induced cirrus.

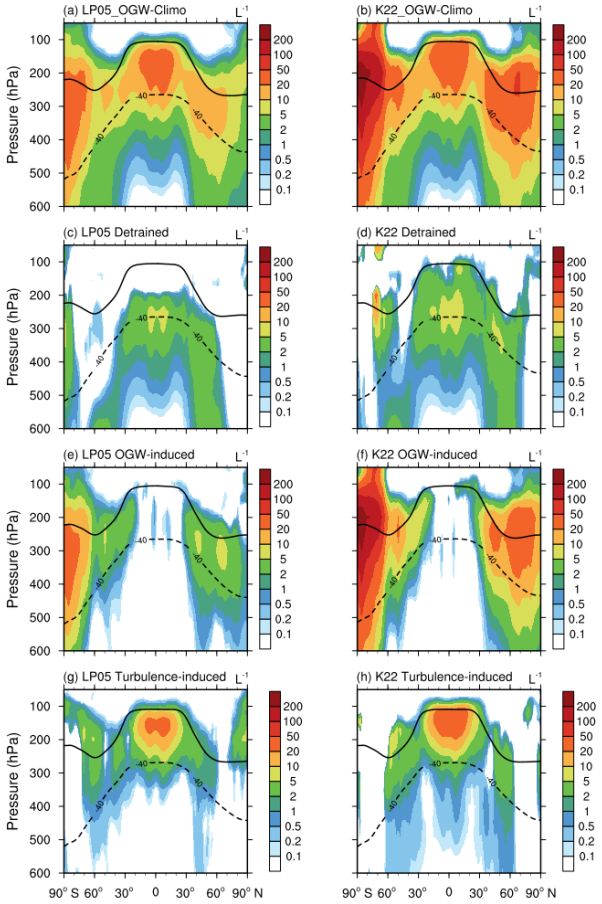

Figure 2. Annual zonal grid-mean ice number concentration (N_i) from 6-year climatology simulations in the upper troposphere (above 600 hPa). The first row shows N_i from the LP05_OGW-Climo and K22_OGW-Climo experiments. The second row shows the differences in N_i between OGW and no_DET experiments (OGW – no_DET) for both the LP05 and K22 schemes, highlighting the contribution from cirrus clouds associated to convective detrainment. The third row presents the N_i differences between OGW and no_OGW experiments (OGW – no_OGW) for both schemes, indicating the presence of orographic cirrus. The fourth row presents the N_i differences between OGW and no_TKE experiments (OGW – no_TKE) for both schemes, reflecting cirrus clouds formed due to turbulence. Dashed lines represent the annual mean -40°C isothermal line, while solid lines indicate the tropopause in the corresponding simulations.

We further analyze grid-mean N_i in the sensitivity tests using homogeneous-only and heterogeneous-only experiments (shown in Fig. 3). These experiments include OGW-induced, turbulence-induced and detrained sources of ice crystals. The results reveal that both nucleation processes produce more ice crystals in the K22 scheme compared to the LP05 scheme. In addition, the N_i ~~results~~ resulting from the OGW-Climo experiments in both the K22 and LP05 schemes closely resembles those from their corresponding OGW-Homo-Climo experiments. This similarity indicates that homogeneous nucleation is a major contributor to the nucleated ice number globally in both the LP05_OGW-Climo and K22_OGW-Climo experiments.

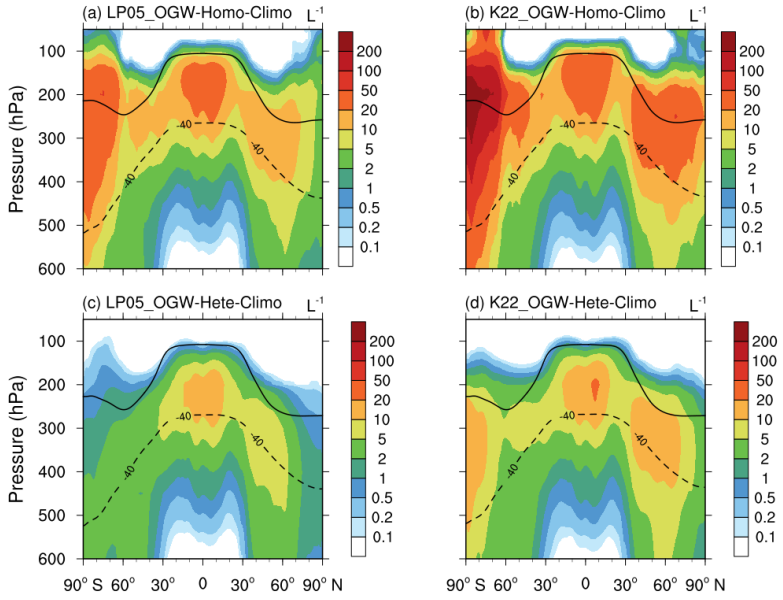

Figure 3. Annual zonal grid-mean N_i from 6-year Climatology simulations in the upper troposphere (above 600 hPa). Dashed lines indicate the annual mean -40 °C isothermal line, and solid lines represent the tropopause in the corresponding simulations.

The K22 scheme simulates ~~The~~ higher activated number concentrations of aqueous aerosols for homogeneous nucleation ~~in the K22 scheme,~~ compared to the LP05 scheme, as shown in Fig. 3a, b~~.~~. This difference can be attributed to both direct and indirect influences. ~~Although the homogeneous nucleation parameterizations in both schemes are based on Koop et al. (2000), t~~The direct effect stems from how each scheme represents the competition of nucleated ~~influence on homogeneously nucleated ice number arises from differences in the competition with~~with pre-existing ice crystals ~~in the two schemes~~. As ~~illustrated~~ described in Section 2.2.3, the number of nucleated ice crystals in the LP05 scheme tends to be more suppressed~~encourage~~ by the competition~~s~~ ~~between~~ with pre-existing ice ~~crystals and newly formed ice crystals~~, compared to the K22 scheme. Consequently, ~~Less~~the presence of pre-existing ice crystals leads to fewer ice crystals that are formed ~~in the LP05 experiments with the existence of pre-existing ice crystals~~, producing overall lower ice number concentrations in the LP05 scheme. The indirect effects are associated with differences in temperatures and vertical velocity fields between the two schemes.

Formatted: Font: (Asian) +Body Asian (宋体), (Asian) Chinese (Simplified, Mainland China)

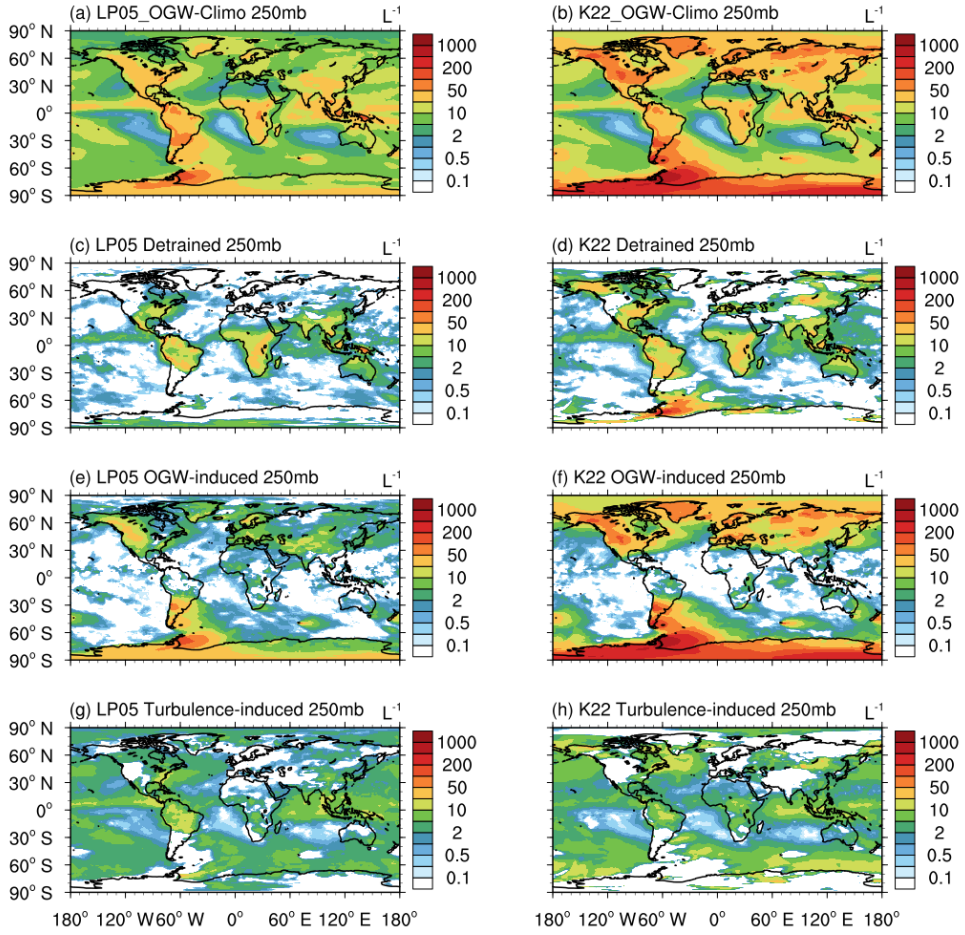

Figure 4. Annual grid-mean N_i from 6-year climatology simulations at 250 hPa. The first row shows N_i from the LP05_OGW-Climo and K22_OGW-Climo experiments. The second row shows the differences in N_i between OGW and no_DET experiments (OGW – no_DET) for both the LP05 and K22 schemes, highlighting the contribution from cirrus clouds associated to convective detrainment. The third row presents the N_i differences between OGW and no_OGW experiments (OGW – no_OGW) for both schemes, indicating the presence of orographic cirrus. The fourth row presents the N_i differences between OGW and no_TKE experiments (OGW – no_TKE) for both schemes, reflecting cirrus clouds formed due to turbulence. ~~Dashed lines represent the annual mean −40°C isothermal line, while solid lines indicate the tropopause in the corresponding simulations.~~

Fig. 4 shows ~~a~~the global longitude-latitude distribution of annual mean N_i at 250 hPa. ~~Consistent with the results shown in Fig. 2, the K22_OGW-Climo experiment tends to produce higher ice number concentrations in all three types of simulated cirrus compared to the LP05_OGW-Climo experiment.~~ In both schemes, cirrus clouds related to convective detrainment are frequently simulated ~~frequently occur~~ over land in low and mid-latitudes~~.~~, while ~~C~~cirrus clouds due to OGWs primarily ~~mostly~~ occur over mountains and highlands in mid- and high latitudes. ~~In addition,~~ Turbulence-induced cirrus clouds ~~due to turbulence~~ exhibit widespread global coverages~~have wide-spread contributions globally~~. ~~C~~Consistent with the results shown in Fig. 2, the K22_OGW-Climo experiment ~~tends to~~ produces higher N_i values ~~ice number concentrations~~ in all three cirrus types ~~of simulated cirrus~~ compared to the LP05_OGW-Climo experiment~~.~~ (Fig. 4a and 4b). While the distribution of detrained N_i appears similar in low latitudes between the two schemes, notable differences emerge in high latitudes, with the K22 scheme generating more ice crystals, particularly over Alaska and the Antarctic Peninsula (Fig. 4c and 4d). OGW-induced ice crystals in the K22 scheme are more abundant and broadly distributed over mountainous regions compared to the LP05 scheme (Fig. 4e and 4f). Additionally, the K22 scheme simulates a higher number of turbulence-induced ice crystals, especially over mid- and high latitude regions (Fig. 4g and 4h). For OGW-induced cirrus clouds, the K22 scheme distributes high N_i values (>100 L^{-1}) more extensively than the LP05 scheme, particularly in mid- and high latitudes. This broader distribution results in a higher cloud frequency in the K22 scheme, as shown in Fig. S1.

~~Notably, the K22 scheme distributes high N_i values (>100 L^{-1}) more broadly than the LP05 scheme, particularly in mid- and high latitudes. The extensive regions with high N_i in the K22_OGW_Climo experiment closely resemble the distribution of cirrus clouds induced by OGWs. This indicates that orographic cirrus clouds are primarily responsible for this shift between the K22 and LP05 schemes. This shift result in a higher cloud frequency in the K22 scheme compared to the LP05 scheme (Fig. S1). As discussed in Section 2.2, the competition between homogeneous nucleation and pre-existing ice is less competitive in the K22 scheme than in the LP05 scheme. This reduced competition leads to increased ice crystal formation, consequently resulting in higher cloud frequency. A further detailed analysis will be presented in the upcoming discussion of the SPARTICUS campaign.~~

~~The difference in ice number between the K22_OGW-Climo and LP05_OGW-Climo experiments is indirectly influenced by changes in temperature and subgrid-scale vertical velocity variance for ice nucleation. Cirrus clouds warm the~~

~~atmosphere below and cool the atmosphere above the cloud layers. In high latitudes, the higher occurrence of cirrus clouds in the upper troposphere results in warming of the lower troposphere and cooling of the stratosphere (Fig. S2). However, the overall indirect impact from temperature changes on ice number is not significant in the troposphere, as the temperature changes are generally small (mostly less than ±0.25 °C).~~

To analyze the factors driving differences in N_i between the LP05 and K22 schemes, several key variables should be considered. These factors include temperature, which affects ice nucleation thresholds and saturation vapor pressure; subgrid-scale vertical velocity, which determines the supersaturation necessary for ice formation; and dust aerosol number concentration, along with the fraction of activated INPs (Φ), which together determine the number of heterogeneously nucleated ice crystals.

In high latitudes, temperature increases in the upper troposphere are found in the K22_OGW-Climo experiment compared to the LP05_OGW-Climo experiment (Fig. S2), likely due to localized warming associated with increased cirrus cloud occurrence (Fig. S1). However, these temperature changes are generally small (typically smaller than ±0.25 °C) and mostly positive, suggesting a suppression of ice nucleation. Therefore, the impact of temperature difference on global N_i is expected to be negative and unlikely to account for a globally significant increase in N_i observed in the K22 scheme (Fig. 2).

Similarly, subgrid-scale vertical velocity increases in the K22_OGW-Climo experiment compared to the LP05_OGW-Climo experiment, particularly in the upper troposphere at mid- and high latitudes (Fig. S3). While these changes may enhance ice nucleation locally, their overall impact on N_i remains limited, as vertical velocity changes are generally small ~~Changes in the tropospheric temperature also impact global circulation, which in turn affects the subgrid-scale vertical velocity variance for ice nucleation, as shown in Fig. S3. In the K22_OGW-Climo experiment, vertical velocity variances increase over mid- and high latitudes in the upper troposphere and lower stratosphere compared to the LP05_OGW-Climo experiment. These enhanced dynamic factors can lead to a higher number of ice crystals through the occurrence of homogeneous nucleation. However, the overall indirect impact from changes in vertical velocity on ice number is small in the troposphere as the changes in vertical velocity are generally small (mostly~~ (less than ±0.002 m s^{-1}) in most regions. Therefore, they are unlikely to explain the globally significant increase in N_i simulated in the K22 scheme (Fig. 2). ~~, except in the mid-latitudes of the Northern Hemisphere.~~

The most substantial differences in N_i between the two schemes arise from microphysical processes, particularly those governing heterogeneous ice nucleation. Both the K22 and LP05 schemes account for the activation of coarse mode dust particles, but the K22 scheme simulates higher dust aerosol number concentrations, especially in the upper troposphere (Fig. S4). This enhancement is likely driven by changes in large scale circulation patterns and surface wind fields resulting from differences in the applied ice nucleation schemes, which influence both dust emission and atmospheric transport. As a result, the K22 scheme shows an increase in ice number concentration nucleated from dust particles heterogeneously, as shown in Fig. 3c and 3d. The activated INP fraction Φ also plays a crucial role in controlling heterogeneous nucleation. While Φ depends on local thermodynamic conditions, such as temperature, vertical velocity, and supersaturation in the LP05 scheme, the K22 scheme simplifies this dependence, with Φ relying on supersaturation only. Differences in the treatment of Φ, combined with elevated dust concentrations in the K22 scheme influence heterogeneous nucleation on coarse mode dust. However, since the number of coarse mode dust is limited (~10-30 L^{-1}) in the upper troposphere (Fig. S4), even if all the dust particles are nucleated heterogeneously to form ice crystals, their contribution to increased N_i will not reach the levels (~100 L^{-1}) observed in the K22 scheme. Therefore, these factors are unlikely to explain the globally significant increase in N_i seen in the K22 scheme compared to the LP05 scheme (Fig. 2a and Fig. 2b). This also implies that competition between preexisting ice and new ice nucleation is a more dominant factor influencing the simulated N_i.

Fig. S5 and Fig. S6 show the annual mean ice number tendency due to heterogeneous nucleation (ΔN_{i_het}) from 6-year climatology simulations, shown as zonal means (Fig. S5) and at 250 hPa (Fig. S6). Both schemes simulate ΔN_{i_het} are concentrated at mid- and high-latitudes in the upper troposphere (Fig. S5a, b), indicating that heterogeneous nucleation is most active in these regions. High ΔN_{i_het} values extend over land and ocean regions (Fig. S6a, b). Compared to the LP05 scheme, the K22 scheme simulates higher ΔN_{i_het} values in mid and high latitude regions. This enhancement aligns with the higher coarse mode dust number in the K22_OGW-climo experiment (Fig. S4). Both schemes show similar ΔN_{i_het} distributions from convective detrainment between no_DET and OGW experiments (Fig. S5c, d and Fig. S6 c, d), indicating that heterogeneous nucleation is not directly influenced by convective detrainment. In contrast, the no_OGWs experiments (Fig. S5e, f and Fig. S6e, f) show pronounced reduction in ΔN_{i_het} in the mid- and high latitudes compared to OGW experiments, revealing the significant role of OGWs in enhancing heterogeneous nucleation. This effect is especially evident

Formatted: Superscript

Formatted: Font: (Asian) +Body Asian (宋体), (Asian) Chinese (Simplified, Mainland China)

Formatted: Font: (Asian) +Body Asian (宋体), (Asian) Chinese (Simplified, Mainland China)

Formatted: Indent: First line: 0.63 cm, Line spacing:

Formatted: Font: (Asian) +Body Asian (宋体), (Asian) Chinese (Simplified, Mainland China)

Formatted: Font: (Asian) +Body Asian (宋体), (Asian) Chinese (Simplified, Mainland China)

Formatted: Font: (Asian) +Body Asian (宋体), (Asian) Chinese (Simplified, Mainland China)

Formatted: Font: (Asian) +Body Asian (宋体), (Asian) Chinese (Simplified, Mainland China)

Formatted: Font: (Asian) +Body Asian (宋体), (Asian) Chinese (Simplified, Mainland China)

Formatted: Font: (Asian) +Body Asian (宋体), (Asian) Chinese (Simplified, Mainland China)

Formatted: Font: (Asian) +Body Asian (宋体), (Asian) Chinese (Simplified, Mainland China)

Formatted: Font: (Asian) +Body Asian (宋体), (Asian) Chinese (Simplified, Mainland China)

Formatted: Font: (Asian) +Body Asian (宋体), (Asian) Chinese (Simplified, Mainland China)

Formatted: Font: (Asian) +Body Asian (宋体), (Asian) Chinese (Simplified, Mainland China)

Formatted: Font: (Asian) +Body Asian (宋体), (Asian) Chinese (Simplified, Mainland China)

Formatted: Font: (Asian) +Body Asian (宋体), (Asian) Chinese (Simplified, Mainland China)

in the K22 scheme, which shows substantial $\Delta N_{\mathrm{i\_het}}$ reductions over continental regions, especially over mountainous areas such as the Himalayas, Andes, Alps and Rockies, indicating a strong sensitivity of heterogeneous ice nucleation to OGWs. The LP05 scheme exhibits more limited changes in $\Delta N_{\mathrm{i\_het}}$, suggesting a weaker enhancement from OGWs. These different results between the two schemes are due to their distinct parameterizations of heterogeneous nucleation. For turbulence-induced $\Delta N_{\mathrm{i\_het}}$ (Fig. S5 g, h and Fig. S6g, h), both the K22_noTKE and LP05_noTKE experiments simulate reduced $\Delta N_{\mathrm{i\_het}}$ compared to their respective OGW-Climo experiments. This result indicates that turbulence reinforces INP activation.

Fig. S7 and Fig. S8 present the zonal mean and 250 hPa ice number tendency due to homogeneous nucleation ($\Delta N_{\mathrm{i\_hom}}$). In both schemes, homogeneous nucleation primarily occurs over high mountains in mid- and high latitudes, as well as in the tropical tropopause layers (TTL). Overall, the K22 scheme produces larger $\Delta N_{\mathrm{i\_hom}}$ compared to LP05. The LP05_no_DET-Climo experiment exhibits enhanced $\Delta N_{\mathrm{i\_hom}}$ in the tropopause (Fig. S7c and S8c), compared to the LP05_OGW-Climo experiment, indicating that convective detrainment suppresses homogeneous nucleation in the LP05 scheme. In contrast, the K22_no_DET-Climo experiment exhibits limited changes compared to the K22_OGW-Climo experiment (Fig. S7d and S8d), indicating that detrainment has a limited effect on homogeneous nucleation in the K22 scheme. Both schemes simulate significantly reduced $\Delta N_{\mathrm{i\_hom}}$ over high mountains compared to the OGW experiments (Fig. S7e, f and S8e, f), emphasizing the role of OGWs in promoting homogeneous nucleation. Similarly, the no_TKE experiments (Fig. S7g, h and S8g, h) produce reduced $\Delta N_{\mathrm{i\_hom}}$ in the TTL for both schemes, revealing that turbulence enhances homogeneous nucleation in this region.

Further insight into the role of aerosol processes in ice nucleation is provided by the K22_OGW_Shan-Climo experiment, which incorporates an improved treatment of aerosol wet removal by convections based on Shan et al. (2021). In this configuration, dust aerosol concentrations are reduced due to more efficient convective scavenging (Fig. S9), particularly in convectively active low latitude regions. The resulting lower dust number concentrations lead to a reduced heterogeneous nucleation rate (Fig. S10 and S11), which can increase the homogeneous nucleation rate due to less competition from heterogeneous nucleation on dust (Fig. S10 and S11). In this case, improvements in aerosol wet removal may help optimize upper tropospheric aerosol concentrations and can leads to a general increase in N_{i} (Fig. S12).

Formatted: Font: (Asian) +Body Asian (宋体), (Asian) Chinese (Simplified, Mainland China)

Formatted: Font: (Asian) +Body Asian (宋体), (Asian) Chinese (Simplified, Mainland China)

Formatted: Font: (Asian) +Body Asian (宋体), (Asian) Chinese (Simplified, Mainland China)

Formatted: Font: (Asian) +Body Asian (宋体), (Asian) Chinese (Simplified, Mainland China)

Formatted: Font: (Asian) +Body Asian (宋体), (Asian) Chinese (Simplified, Mainland China)

Formatted: Font: (Asian) +Body Asian (宋体), (Asian) Chinese (Simplified, Mainland China)

Formatted: Font: (Asian) +Body Asian (宋体), (Asian) Chinese (Simplified, Mainland China)

Formatted: Font: (Asian) +Body Asian (宋体), (Asian) Chinese (Simplified, Mainland China)

Formatted: Font: (Asian) +Body Asian (宋体), (Asian) Chinese (Simplified, Mainland China)

Formatted: Font: (Asian) +Body Asian (宋体), (Asian) Chinese (Simplified, Mainland China)

Formatted: Font: (Asian) +Body Asian (宋体), (Asian) Chinese (Simplified, Mainland China)

Formatted: Font: (Asian) +Body Asian (宋体), (Asian) Chinese (Simplified, Mainland China)

Formatted: Font: (Asian) +Body Asian (宋体), (Asian) Chinese (Simplified, Mainland China)

Formatted: Font: (Asian) +Body Asian (宋体), (Asian) Chinese (Simplified, Mainland China)

Formatted: Font: (Asian) +Body Asian (宋体), (Asian) Chinese (Simplified, Mainland China)

Formatted: Font: (Asian) +Body Asian (宋体), (Asian) Chinese (Simplified, Mainland China)

Formatted: Font: (Asian) +Body Asian (宋体), (Asian) Chinese (Simplified, Mainland China)

Formatted ...

Formatted ...

Formatted ...

Formatted ...

Formatted ...

Formatted ...

Formatted ...

Formatted ...

Formatted ...

Formatted ...

Formatted ...

~~In the K22 ice nucleation scheme, the difference in heterogeneous nucleation can be attributed to several other factors beyond changes in vertical velocity variances. These include the parameters used for the activated INP fraction, Φ, and the dust number concentration in simulations. Both the K22 and LP05 schemes account for the activation of coarse mode dust particles for heterogeneous nucleation.~~

~~In the K22 experiments, simulated dust aerosol number concentrations tend to be higher compared to those in the LP05 experiment, as depicted in Fig. S4. This difference may stem from changes in the general circulation due to the application of different nucleation schemes. Changes in surface winds may influence dust emissions, while changes in wind fields at different altitudes can influence dust transport and deposition. The increased simulated dust aerosol number concentration in the K22 scheme results in the more ice crystals nucleated heterogeneously compared to the LP05 scheme (Fig. 3c and 3d).~~

~~In CAM6, there is an identified bias of aerosols in the upper troposphere related to the wet removal of aerosols by convections, as highlighted by Shan et al. (2021). Fig. S5 and S6 illustrate the N_i and mass-weighted number concentrations of coarse mode dust in the K22_OGW_Shan experiment. With improved aerosol wet removal by convections, the dust aerosol concentration in the K22_OGW_Shan experiment has been reduced (Fig. S6). As a result, ice crystals due to heterogeneous nucleation has decreased, leading to less suppression of homogeneous nucleation. This enhances the homogeneous nucleation, and thus leads to an increase in N_i (Fig. S5). The improved aerosol wet removal by convection based on Shan et al. (2021) appears to effectively optimize the dust number concentrations under the K22 configuration.~~When the ice nucleation scheme is switched from LP05 to K22, grid-averaged N_i increases in the mid- and high latitudes (Fig. S13a). Ice water content (IWC) also increases (Fig. S13b) especially over high mountains. Ice effective radius (AREI) over land tends to be smaller and AREI over ocean tends to be larger, compared to the LP05 scheme (Fig. S13c). In mid- and high latitudes, longwave cloud forcing (LWCF) is increased over high mountains, as can be seen in Fig. S13d. These changes can be explained by changes in the N_i (Fig. S13h), as the K22 scheme generally simulates more ice crystals over high mountains. Interestingly, negative LWCF can be found over oceans at mid- and high latitudes. This phenomenon is primarily associated with the dominance of optically thin cirrus clouds formed via in-situ nucleation in these regions, as previously reported (Sassen & Cho, 1992; Sassen et al., 2008; Wang et al., 1996; Winker & Wielicki, 2010). The K22 scheme tends to enhance the spatial extent and occurrence frequency of such clouds. Over oceans, where vertical

Formatted: Indent: First line: 0.63 cm, Line spacing:

Formatted: Font color: Auto, Not Highlight

Formatted: Font color: Auto, Not Highlight

Formatted: Font color: Auto, Not Highlight

Formatted: Font color: Auto, Not Highlight

Formatted: Font color: Auto, Not Highlight

Formatted: Not Highlight

Formatted: Not Highlight

velocities are weaker than over land, these optically thin clouds become even thinner. This allows more longwave radiation to space, resulting in negative LWCF over oceans, consistent with the previous findings (Muri et al., 2014; Spang et al., 2024). Shortwave cloud forcing (SWCF) increases in mid- and high latitudes (Fig. S13c), as the shortwave albedo of extensive cirrus clouds (10-40%) is lower than that of the underlying surface (ranging from 50-80% for oceans at low solar angles and 80-90% for snow-covered land). Changes in SWCF, LWCF and net cloud forcing (net CF) caused by the switch of ice nucleation scheme is -0.51 W m^{-2}, 2.95 W m^{-2}, and 2.44 W m^{-2}, respectively. The change in the cloud radiative forcing may influence global temperature, which can modify large-scale circulation and sub-grid turbulence, subsequently affect ice nucleation, cloud frequency, and cloud radiative forcing, and have important implications for high cloud feedbacks (Murray & Liu, 2022).

Formatted: Not Highlight
Formatted: Font color: Auto, Not Highlight
Formatted: Not Highlight
Formatted: Font color: Auto, Not Highlight
Formatted: Not Highlight
Formatted: Font color: Auto, Not Highlight
Formatted: Font color: Auto
Formatted: Font color: Auto, Not Highlight
Formatted: Font color: Auto, Not Highlight
Formatted: Font color: Auto
Formatted: Superscript
Formatted: Superscript
Formatted: Superscript
Formatted: Font color: Auto
Formatted: English (United States)

4.2 SPARTICUS Experiments

Fig. 5a presents the simulated N_i in orographic cirrus during the SPARTICUS campaign for both the LP05_OGW-SP and K22_OGW-SP experiments. ~~Together~~ Together with simulated ~~microphysical properties (~~IWC and D_{num}~~)~~ (Fig. ~~S7~~S14), both ~~experiments~~ schemes produce results that ~~roughly~~ generally agree with observational data. ~~However, t~~The simulated IWC and N_i in the K22_OGW-SP experiment tend to be larger, while D_{num} tends to be smaller, ~~than those in~~compared with the LP05_OGW-SP experiment. This suggests that the K22 scheme simulates more, but smaller ice crystals. Fig. 5b shows the differences ~~of~~ in simulated N_i between the reference experiments (OGW) and sensitivity experiments (no_OGW, no_DET and no_TKE). Larger differences in simulated N_i between sensitivity experiments and the reference experiments indicate a more significant contribution from a respective ice crystal source (OGW-induced, detrained, or turbulence-induced). Specifically, increase or decrease of microphysical properties in the sensitivity experiments compared to the reference experiments reveals how each source contributes to enhancing or ~~inhibits~~ inhibiting the overall ice number concentrations.

Formatted: Font: (Asian) +Body Asian (宋体), (Asian) Chinese (Simplified, Mainland China)

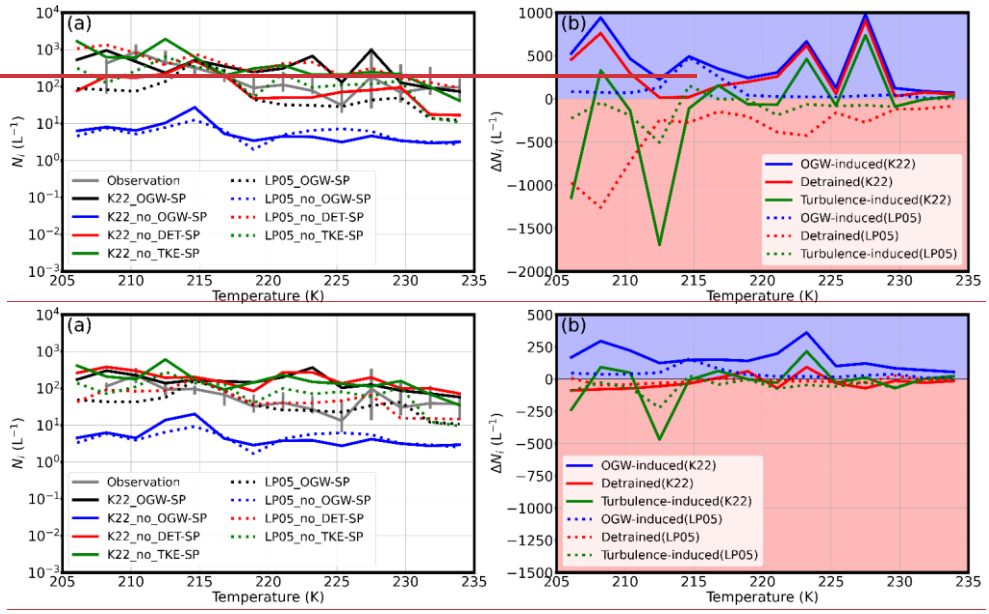

Figure 5. (a) Comparison of N_i between observations and experiments and (b) differences in median N_i values (ΔN_i) between sensitivity tests (no_OGW, no_DET and no_TKE) and reference experiments (OGW) in LP05 and K22 schemes during the SPARTICUS campaign. In panel (a), solid lines represent median N_i values from K22 experiments, while dotted lines represent those from LP05 experiments. The bars indicate observed N_i values, ranging from the 25th percentile to the 75th percentile. In panel (b), the number of ice crystals due to OGW is calculated as N_i in OGW experiments minus N_i in no_OGW experiments. The number of ice crystals from convection detrainment is calculated as N_i in OGW experiments minus N_i in no_DET experiments. The number of ice crystals due to turbulence is calculated as N_i in OGW experiments minus N_i in no_TKE experiments. The blue shaded region indicates that the ice crystal source contributes to N_i and increases N_i in the reference experiments. The red shaded region indicates that the ice crystal source competes with other sources and inhibits N_i in the reference experiments.

Fig. 5b ~~demonstrates~~ shows that in both LP05 and K22 schemes, the changes in N_i (ΔN_i) due to OGWs are always positive and larger than those from the other two sources in these cirrus clouds. This indicates that OGWs ~~make~~ play a significant role ~~contributions~~ in enhancing~~to~~ the formation of ice crystals in cirrus clouds identified as orographic cirrus

during the observed five-days period. Particularly in regions with temperatures below 215 K, where both schemes simulate their highest N_i peaks, ΔN_i due to OGWs ~~also~~ peaks positively at the corresponding temperatures. This suggests that OGW-induced ice crystals ~~are significant contributors to the ice crystals~~ enhance the overall N_i in these cirrus clouds.

Detrained and turbulence-induced ΔN_i values show different signs, fluctuating between positive and negative at different temperatures, indicating that ~~T~~the effects of the other two sources ~~are different~~are uncertain and vary between the two schemes. In the LP05 scheme, detrained and turbulence-induced ΔN_i values are generally negative, suggesting that ice crystals from both detrainment and turbulence tend to ~~have~~ inhibit~~ion effects on~~ N_i. In contrast, the K22 scheme exhibits varied signs of detrained and turbulence-induced ΔN_i values, with stronger fluctuations between positive and negative, ~~shows~~indicating that these sources can either enhance or inhibit N_i. ~~clear contributions from detrained ice crystals and varied effects (both contribution and inhibition) from turbulence-induced ice crystals~~. Notably, the positive ΔN_i values in detrained and turbulence-induced ice crystals are smaller in the LP05 scheme, suggesting stronger competition (inhibition effects) between ice sources in the LP05 scheme. ~~These differences arise from the distinct representations of competing ice sources between the two schemes.~~

~~However, in the high-temperature regions (T>220 K) shown in Fig. 5b, differences in ΔN_i between the LP05 and K22 schemes are more pronounced. In the LP05 scheme, ΔN_i due to turbulence and detrainment is generally negative, indicating inhibition effects on N_i. On the contrary, the K22 scheme simulates positive ΔN_i values from these two ice sources, suggesting their contributing effects.~~

Regarding the simulated number weighted diameter of ice crystals (D_{num}) in the LP05 and K22 experiments (Fig. ~~S~~S15~~8~~ and ~~S~~S16~~9~~), the no_OGW experiments ~~generate~~ produce the largest D_{num} ~~in the~~ among all experiments. This implies that ice crystals nucleated due to OGW tend to have the smallest D_{num} in the simulations. ~~On the contrary, the smallest D_{num} in the LP05_no_DET_SP experiment indicates that detrained ice crystals contributed the most to the increase in ice crystal sizes. This is consistent with the fixed diameters of 50 μm for detrained ice crystals in the simulations. However, the K22_no_DET_SP experiment does not show similar changes in D_{num} as simulated in the LP05_no_DET_SP experiment. In the LP05 scheme, ice crystals from the detrainment compete for water vapor with the OGW-induced small ice crystals,~~

Formatted: Font: (Default) +Headings (Times New Roman)

Formatted: Font: (Default) +Headings (Times New Roman)

which is the dominant ice source. The larger detrained ice crystals thus have more opportunity to manifest their size characteristics, increasing the overall D_{num} in the LP05_OGW-SP experiment. This competitive effect is evident when comparing the LP05_OGW-SP experiment with the sensitivity experiment without detrainment (LP05_no_DET-SP), which shows a smaller D_{num}, highlighting the dominance of small, nucleated ice crystals from OGWs.

In contrast, in the K22 scheme, the detrained ice crystals do not face significant competition. Consequently, the "large-size" characteristics of these detrained ice crystals are less apparent between the reference experiment (K22_OGW-SP) and sensitivity experiment (K22_no_DET-SP).

Fig. S7 reveals that the K22_OGW-SP experiment generates smaller number-weighted diameters (D_{num}) than the LP05_OGW-SP experiment. The combination of smaller D_{num} and larger N_i in the K22_OGW-SP experiment suggests that the K22 scheme tends to produce cirrus clouds with a higher number of smaller ice crystals. This characteristic helps explain why the K22 scheme results in increased cloud frequency compared to the LP05 scheme. The above analysis of D_{num} highlights the importance of properly parameterizing detrained ice size and competition of ice for water vapor between different sources. Inappropriate settings for detrained ice size can negatively influence the microphysical properties of cirrus clouds. This is especially crucial in models where competition between detrained ice crystals and nucleated ice crystals affects the overall cloud characteristics. Ensuring that these parameters are appropriately represented is essential to reproduce observed characteristics of cirrus clouds microphysics and associated climate effects.

Formatted: Indent: First line: 0.63 cm

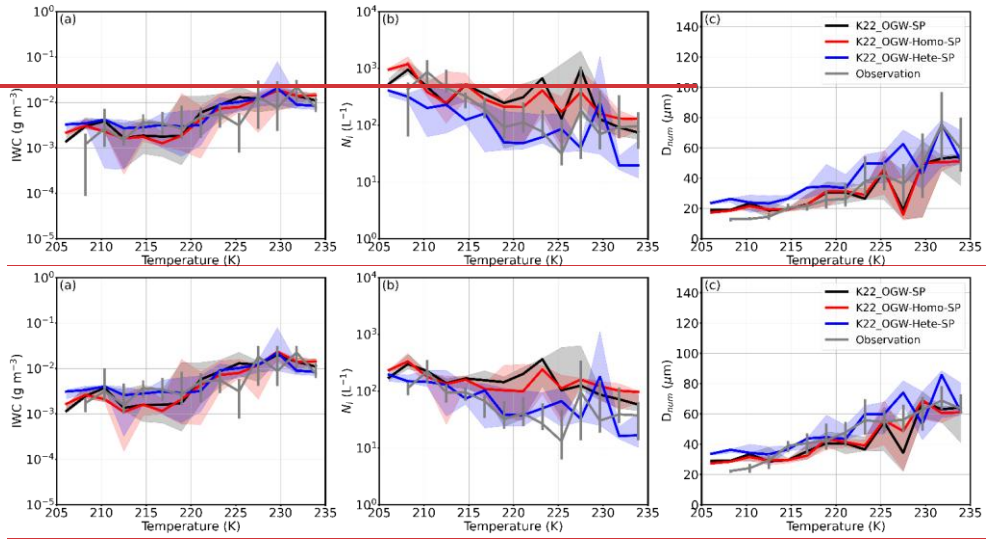

Figure 6. Comparison of IWC (a), N_i (b) and D_{num} (c) with respect to temperature between observations and K22 sensitivity experiments (K22_OGW, K22_OGW-Homo-SP and K22_OGW-Hete-SP) for orographic cirrus (5 days) during the SPARTICUS campaign.

A detailed analysis of sensitivity tests with the K22 scheme for ~~the~~ simulati~~ng~~ons ~~of~~ orographic cirrus clouds has been conducted. As depicted in Fig. 6, the microphysical properties (IWC, N_i and D_{num}) in the K22_OGW-SP experiment closely align with those in the K22_OGW-Homo-SP experiment. This ~~alignment~~ similarity suggests that homogeneous nucleation is the dominant mechanism for ~~simulating~~ orographic cirrus during the SPARTICUS campaign using the K22 scheme. This finding is consistent with the results of Lyu et al. (2023) using the LP05 scheme, who also identified the homogeneous nucleation as the dominant mechanism for ice nucleation in orographic cirrus during the SPARTICUS campaign. ~~–~~The simulated coarse mode dust number concentrations are shown in Fig. S17, which shows higher values in the K22 scheme than those in the LP05 scheme. However, the dust concentrations are very low (<1 L_a^{-1}) in both schemes, which supports the dominance of homogeneous nucleation for cirrus cloud formation during the SPARTICUS campaign.

Formatted: Superscript

Furthermore, comparing simulation results with observations, the microphysical properties in the K22_OGW-Hete-SP experiment show closer agreement with the observations than those in the other two experiments (Figure 6). This is largely due to the use of a 20-μm size cut threshold, which filters out many small ice crystals typically associated with homogeneous nucleation. This interpretation is supported by the 10-μm size cut results (Fig. S18), where the inclusion of data from the less reliable first size bin captures more small ice crystals, characteristic of homogeneous nucleation, leading to better agreement of D_{eum} between observations and the K22_OGW-Homo-SP and K22_OGW-SP experiments. Additionally, discrepancies between the simulations and observations may stem from limitations in model representations of other microphysical processes, such as ice depositional growth, cloud ice to snow autoconversion, and accretion, and ice sedimentation.

Formatted: Font: Italic

Formatted: Subscript

Formatted: Font: (Asian) +Body Asian (宋体), (Asian) Chinese (Simplified, Mainland China)

4.3 ORCAS Experiments

In Region 1, ~~the median values of~~ both simulated and observed median values of IWC are typically low, ~~at~~around 10^{-3} g m^{-3}, implying that less water vapor is available for ice formation ~~in continental environments~~. The dataset used in the analysis includes 83559 data points. As shown in Fig. 7, the median ~~values of~~ simulated N_i generally hover around 3 L^{-1}, which is close to the upper limit of observed N_i. range. However, ~~S~~simulated N_i tends~~are~~ to be~~often~~ overestimated, except near~~around~~ 225 K, where they are slightly underestimated compared to observations. The simulated coarse mode dust number concentrations are presented in Fig. S19, which shows higher values with the K22 scheme compared to the LP05 scheme.

Formatted: Font: (Asian) +Body Asian (宋体), (Asian) Chinese (Simplified, Mainland China)

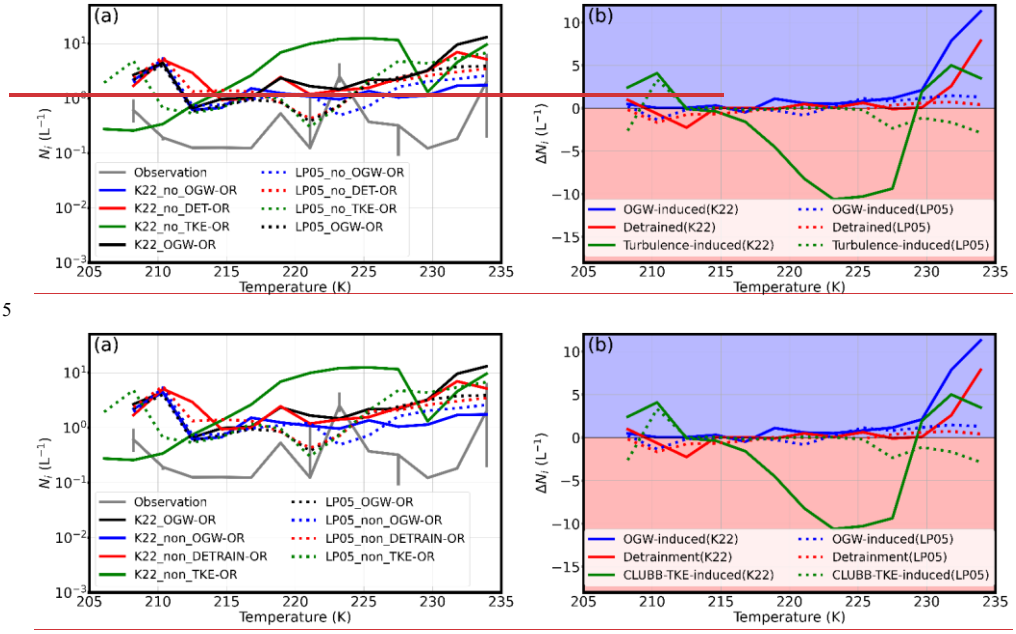

Figure 7. Same as Figure 5 but for cirrus clouds during the ORCAS campaign in Region 1.

~~Regarding observed N_i, a~~As shown in Fig. 7, multiple observed N_i peaks correspond to different contributors to ΔN_i, revealing that cirrus clouds exhibit multilayer structures with distinct ice sources. ~~There are pronounced peaks in~~ Ssimulated N_i displays pronounced peaks above 225 K and near 210 K ~~and high N_i values at temperatures above 225 K~~. At the ~~lower altitudes~~ ~~levels~~, where high N_i values are observed at temperatures above 225 K, ~~simulated~~ both schemes simulate positive ΔN_i values, indicating that ice crystals due to OGWs and detrainment are ~~contribute the most~~ the dominant contributors to simulated N_i in both ~~the LP05 and K22~~ schemes. In the LP05 scheme, turbulence-induced ΔN_i values are generally negative, implying that ~~I~~ice crystals from turbulence tend to suppress the overall ~~exhibit inhibiting effects on simulated N_i in the LP05 scheme~~. ~~while~~In contrast, in the K22 scheme, ~~they~~ turbulence-induced ΔN_i values fluctuate from negative to positive ~~show~~

~~varying effects, with~~suggesting inhibition between 215-230 K and ~~contribution~~enhancement ~~to simulated N_i~~ at temperatures ≥ 235 K.

At the 210 K level, the overwhelmingly positive ΔN_i values due to turbulence in both schemes suggest that~~simulated~~ turbulence-induced ice crystals ~~due to turbulence~~ are the primary contributor~~s~~ to N_i ~~in both schemes~~ (Fig. 7b). However, in the LP05 scheme, ~~ice crystals~~ΔN_i values due to OGWs ~~and detrainment~~ are negative, suggesting that OGW-induced ice crystals tend to inhibit ~~the~~ ice crystal formation ~~of simulated N_i~~. In contrast, their impacts are minimal (~0) in the K22 scheme. In addition, both schemes simulate generally negative ΔN_i values due to detrainment, implying that detrained ice crystals tend to suppress the following ice formation.~~, whereas their effects are minimal in the K22 scheme.~~

~~At the lower levels, where high N_i values are observed at temperatures above 225 K, simulated ice crystals due to OGWs and detrainment contribute the most to simulated N_i in both the LP05 and K22 schemes. Ice crystals from turbulence exhibit inhibiting effects on simulated N_i in the LP05 scheme, while in the K22 scheme, they show varying effects, with inhibition between 215-230 K and contribution to simulated N_i at temperatures ≥ 235 K.~~

Region 2, located downwind of the southern end of South America and the Antarctic peninsula, features a narrow landmass extending into the sea. These high-lands create unique conditions for cirrus clouds, characterized by high vertical velocities ~~and relatively high levels of water vapor~~. The dataset used in the analysis includes 146139 data points. The observed median IWC values in Region 2 remain~~stay~~ close to 10^{-2} g m^{-3}, indicating a relatively moist environment ~~over the oceans~~. Figure S20 shows the simulated coarse mode dust number concentrations, with the K22 scheme generally simulating higher dust concentrations compared to the LP05 scheme.

Formatted: Indent: First line: 0 cm

Formatted: Font: (Asian) +Body Asian (宋体), (Asian) Chinese (Simplified, Mainland China)

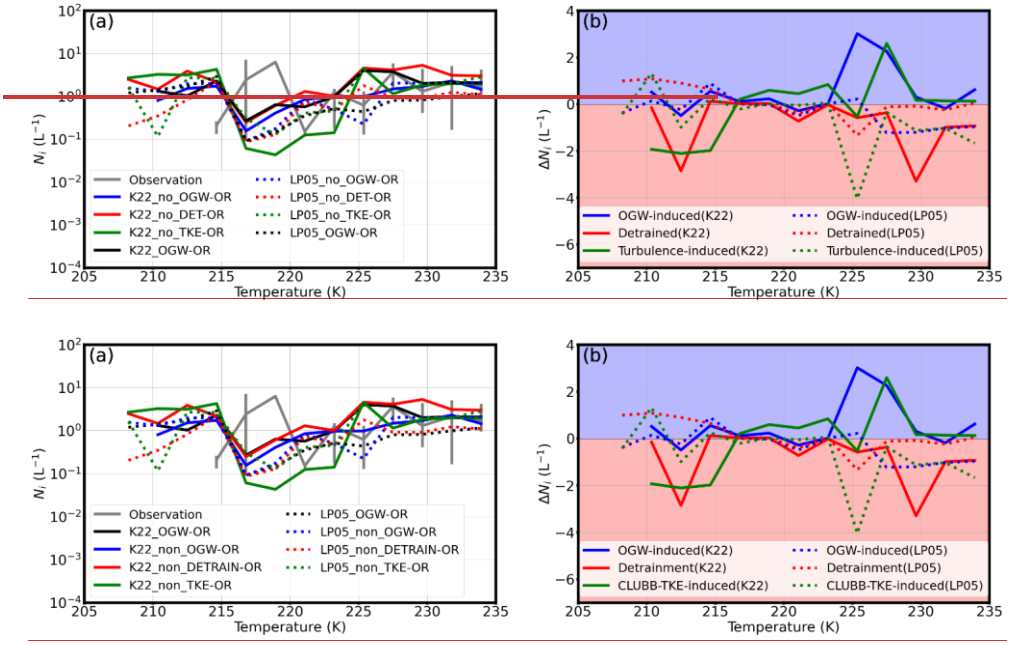

Figure 8. Same as Figure 7 except in Region 2.

In Fig. 8a, similar to Region 1, multiple high N_i peaks again correspond to different primary ΔN_i contributors, ~~both observed and simulated N_i show that all experiments (OGW, no_DET, no_OGW and no_TKE) successfully capture the high N_i peaks with~~ suggesting multilayer structures of cirrus clouds in Region 2~~s~~. ~~For the high N_i peaks near 215 K,~~ Near 215 K, the OGW experiments in~~ produce the~~ both schemes simulate high~~est~~ N_i peaks~~,~~ ~~–~~ that closely match~~ing~~ the ~~observed magnitude~~observed peak near 218 K. The corresponding positive OGW-induced ΔN_i values in both schemes (Fig. 8b) suggest~~s~~ that a large portion of these ice crystals ~~contributing to these peaks~~ are ~~predominantly~~ generated by~~from~~ OGWs originating from~~by~~ mountains and high plateaus ~~in both the LP05 and K22 schemes~~. The contributions from other sources (detrainment and turbulence) differ~~s~~ between the two schemes~~:~~. In the LP05 scheme, generally positive detrained ΔN_i and fluctuating turbulence-induced ΔN_i near 215K ~~shows a preference for contributions from turbulence and detrainment~~suggest

an enhancement role ,from detrainment and a mix of enhancement and inhibition effects from turbulence. ~~whereas~~In contrast, ~~ ~~the K22 scheme exhibits negative ΔN_i values ~~tends to display~~for both sources, indicating overall ~~the~~ inhibition effects. The~~se~~~~is~~ findings ~~imply~~~~suggests~~ that ~~simulated~~the N_i peaks around 215 K are strongly related to the mountainous terrain upwind of Region 2.

Notably, while ~~the~~ simulated N_i peaks are around 215 K, the observed N_i peak occurs around 219 K. This bias may be due to an underestimation of ice crystal fall speeds in the model, ~~which could result from either~~potentially caused by ~~the~~ slow growth of simulated ice crystals or biases in the fall speed parameterization ~~of ice crystal fall speed~~. The broader spatial distribution of ice crystals in the K22 scheme leads to stronger competition among multiple ice sources ~~in the K22 scheme is due to the wider spread of ice crystals~~. In contrast, in the LP05 scheme, ~~the~~ OGW-induced ice crystals tend to remain concentrated over mountainous areas~~s~~, (as shown in Fig. 4)~~.~~ ~~This~~ results~~ing~~ in ~~a~~ more localized effects. In the K22 scheme, however, ~~the wider spread of~~ the high N_i ~~ice crystals~~(>100 L^{-1}) extends over a larger area, facilitating~~allows~~ ~~for~~ interaction and competition ~~among different~~ between OGW-induced ice sources and other ice sources, even far~~at greater distances~~ from the mountainous regions~~s~~.

In the lower part of cirrus clouds ~~below the 225 K level~~ (T > 225K), negative ΔN_i values of all three ice crystal sources in the LP05 scheme suggest~~show~~ universal competition ~~in the LP05 scheme~~ among these sources. In contrast, in the K22 scheme, ~~ shows less competition among these sources~~ only detrained ΔN_i values are negative, suggesting inhibition effects~~.~~ ~~,~~ while ΔN_i values from OGWs and turbulence are positive, ~~In the K22 scheme~~suggesting~~, ice crystals due to OGWs and turbulence~~ enhancement effects~~contribute positively to simulated N_i, and only detrained ice crystals exhibit inhibition effects~~. The fact that no ΔN_i values from a single source are overall positive in both schemes may suggest that ~~Both schemes fail to simulate the same~~the dominant ice source is missing from the model~~, indicating the absence of dominant ice sources in these simulations~~. Previous studies have ~~shown~~ highlighted the importance of additional ice nucleation sources, ~~that frontal waves~~such as frontal gravity waves, in~~are important dynamic factors for~~ the cirrus formation over oceans, and identified~~while~~ crucial INPs includ~~ing~~e dust, metallic particles, soot and biological materials (Fan et al., 2016; Froyd et al., 2022; Heymsfield et al., 2017; Kärcher & Ström, 2003; Knopf & Alpert, 2023). However, ~~I~~in CAM6, ~~however, frontal~~only OGWs ~~gravity waves~~ are ~~not~~ included in the ice nucleation ~~processes~~, and only coarse mode dust is considered as INPs. In

addition, other important N_i source and sink processes, such as secondary ice production, ice sublimation and sedimentation should be examined. ~~.~~ Future studies are therefore necessary to incorporate these potential~~missing~~ ~~ice~~dynamic and microphysical sources ~~into the model~~ to improve simulations of cirrus clouds over oceanic regions.~~s.~~

In Region 3, the observed median IWC ~~median~~ values are even higher than those in Region 2, with maximum values reaching up to 10^{-1} g m^{-3}. This suggests a water vapor-rich environment for cirrus clouds in this region. There are 111712 data points used in the analysis. ~~In addition, the observed N_i displays~~ Multiple high N_i peaks with different primary contributors reveal~~a~~ multilayer structures of cirrus clouds, similar to Regions 1 and 2 (Fig. 9). Simulated coarse mode dust number concentrations from both schemes are compared in Fig. S21, showing that the K22 scheme simulates much higher dust concentrations than the LP05 scheme.

Formatted: Font: (Asian) +Body Asian (宋体), (Asian) Chinese (Simplified, Mainland China)

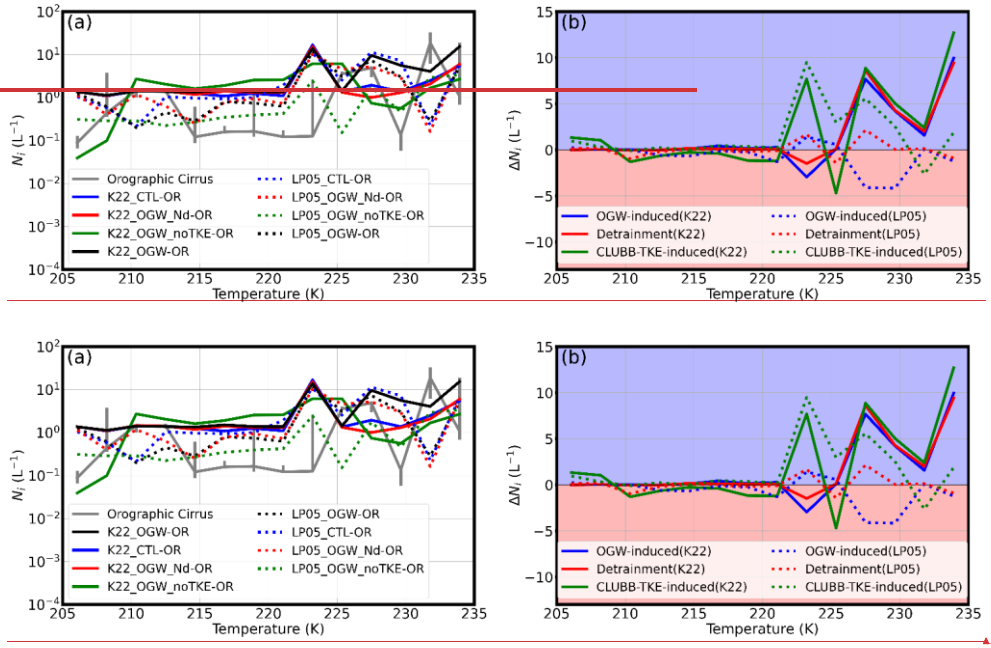

Figure 9. Same as Figure 7 except in Region 3.

In higher-level cirrus clouds (T < 220 K), both simulated and observed median N_i ~~median~~ values are ~~small~~low, ~~typically~~usually less than 1 L^{-1}. ~~This indicates weak vertical wind speeds in the oceanic environment. At the cloud top, ice crystals due to turbulence make the most contributions to the simulated N_i peaks when T < 210 K in both schemes (Fig. 9b).~~ However, the simulated N_i in both schemes shows poor agreement with observations~~, suggesting~~ This discrepancy may result from the inability of~~that turbulence from CLUBB TKE~~the model ~~struggles~~ to capture~~simulate~~ the realistic dynamic factors necessary for ~~realistic~~ ice nucleation~~, such as gravity waves~~ (Gasparini et al., 2023; Kärcher & Podglajen, 2019). The absence of ~~actual~~ observed ice sources in the simulation points to potentially missing dynamic factors, such as frontal ~~gravity waves~~ or convective gravity waves, which are likely key drivers of~~responsible for~~ ice nucleation under these conditions. At

Formatted: Font: (Asian) +Body Asian (宋体), (Asian) Chinese (Simplified, Mainland China)

low temperature levels (T < 209 K), both schemes exhibit positive turbulence-induced ΔN_i values, suggesting that ice crystals due to turbulence make the most contribution to N_i at these cold temperatures (Fig. 9b).

In the lower levels of cirrus clouds (T > 227 K), ~~M~~most of ~~high~~ the simulated N_i ~~values peaks are occur in the lower levels of cirrus (T > 223 K)~~ (Fig. 9a). At these temperatures, turbulence-induced ΔN_i values are mostly positive and generally exceed OGW-induced and detrained ΔN_i values~~.~~ in both schemes, suggesting ~~Both schemes simulate~~a strong ~~contributions~~ enhancement of N_i from turbulence~~-induced ice crystals.~~. However, OGW-induced and detrained ΔN_i values differ between the two schemes. ~~but they differ in the effects of ice sources due to OGWs and detrainment.~~ In the K22 scheme, positive OGW-induced and detrained ΔN_i values ~~The K22 scheme~~suggest ~~simulates a significant greater contribution~~enhancements to N_i from ~~ice crystals due to~~ OGWs and detrainment. In contrast,~~,~~ ~~while~~the LP05 scheme shows large variability, with OGW-induced and detrained ΔN_i values ~~the LP05 scheme~~fluctuating between positive and negative, indicating ~~provides more varied~~ more complex and varied effects from~~of~~ these ice sources in the simulations.~~.~~

~~4.4~~ Numerous studies have demonstrated that turbulence from CLUBB-TKE can hardly predict perturbations from gravity waves (Golaz et al., 2002a, 2002b; Huang et al., 2020). To accurately simulate cirrus clouds over oceans in Region 3, it is necessary to incorporate representations of other key dynamic drivers for ice nucleation, such as frontal and convective gravity waves. It is also important to incorporate key INPs (e.g., marine organic aerosols) besides mineral dust into ice nucleation schemes. Other source and sink terms beyond ice nucleation, such as secondary ice production, ice sublimation, and sedimentation, may also play a significant role in influencing the N_i evolution over oceans.

~~Numerous studies have demonstrated that turbulence from CLUBB-TKE can hardly predict perturbations from gravity waves (Golaz et al., 2002a, 2002b; Huang et al., 2020). Consequently, ice crystals generated by turbulence and from convective detrainment fail to account for critical ice sources over oceans, especially those associated with gravity waves such as frontal and convective gravity waves. To accurately simulate cirrus clouds over oceans, it is necessary to incorporate representations of these key dynamic factors driving ice nucleation.~~

Formatted: Font: Not Italic

Formatted: Font: Not Italic

Formatted: Font: Not Italic

Formatted: Indent: First line: 0.63 cm, Line spacing:

~~To improve the model's performance in simulating cirrus microphysical properties over oceans, it is also important to incorporate key INPs into ice nucleation schemes. Previous studies have shown that heterogeneous nucleation plays a significant role over oceans, with mineral dust and metallic particles acting as important INPs (Cziczo et al., 2013; Froyd et al., 2022). Furthermore, soot and biological materials have also been identified (Fan et al., 2016). Including these aerosols may improve the simulation of cirrus clouds by the model.~~

~~4.5~~4.4 Implication of different behaviours in ice sources with the two nucleation schemes

Both K22 and LP05 schemes can effectively simulate the ice nucleation as ~~the~~a dominant ice source~~s~~ in orographic cirrus clouds, ~~but~~ though they ~~show~~ exhibit different influences~~effects~~ from ~~the~~ minor ice sources on simulated ~~high~~ N_i. ~~For instance, in orographic cirrus, b~~In both schemes, ~~simulate~~ OGW-induced ice crystals emerge as the dominant contributors, while detrained and turbulence-induced ice crystals show varying effects as minor ice sources. This distinction is useful to identify cirrus types observed during the flight campaigns. ~~Since both schemes can simulate orographic cirrus clouds, we use these clouds observed~~To test this method, we identify orographic cirrus clouds during the SPARTICUS campaign by examining cases where OGW-induced ice source dominates in the simulations and the simulated N_i aligns closely with observations in both schemes. ~~as a case study to test this method.~~

~~The flight dates when OGW-induce ice sources dominate in the simulations and the simulated N_i aligns closely with observations include~~ This analysis yields 16 such flight days: January 26, 27, February 10, 17, 19, 20, March 14, 17, 19, 30, April 1, 11, 12, 19, 28, and 29. Among these days, 5 days (March 19, 30, April 1, 28 and 29) correspond to previously identified orographic cirrus events reported by ~~Our method successfully identifies the orographic cirrus observed by~~ Muhlbauer, Ackerman, et al. (2014). ~~Orographic cirrus, referred to as ridge-crest cirrus in their study, are identified on: March 19, 30, April 1, 28 and 29. During these days, OGW-induced ice crystals are the dominant ice sources. Furthermore, we expanded our identification to include 16 days of flight, compared to the 5 days in Muhlbauer, Ackerman, et al. (2014).~~ ~~This~~ By expanding the previously identified orographic cirrus days, ~~extension increases~~ the number of available data points increases from 6236 to 15454, thereby enhancing~~making the results more convincing~~ robustness and credibility of our analysis.

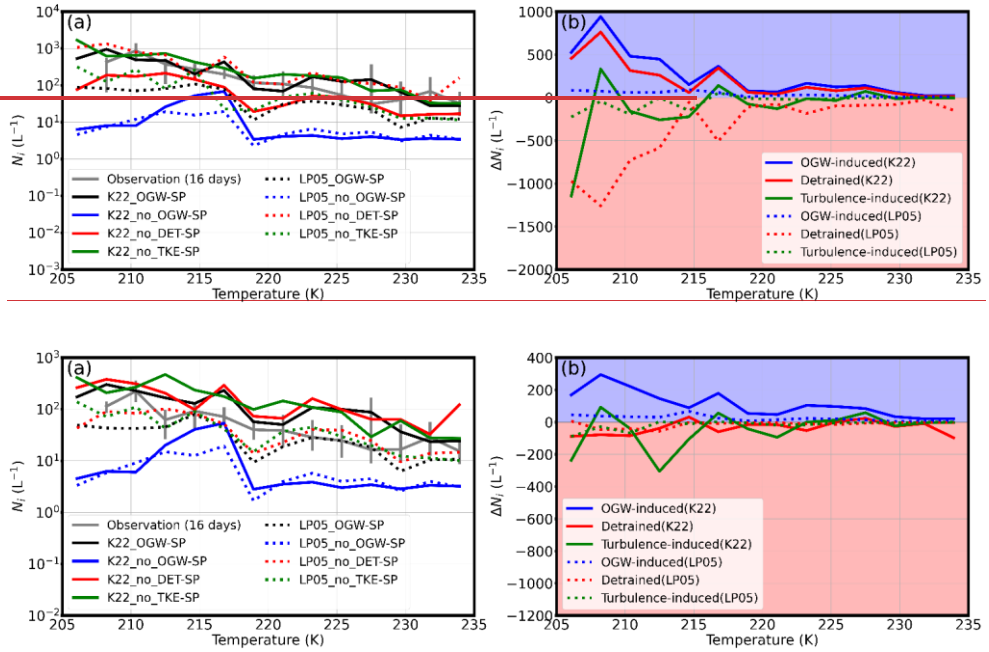

Figure 10. Same as Figure 5 except for identified orographic cirrus by our approach (16 days of flights).

Fig. 10 illustrates the microphysical properties of identified orographic cirrus over the 16-day period using our approach. Both schemes simulate N_i values that are in reasonable agreement with the observations. The N_i values in K22_OGW-SP experiment are generally larger than those in the LP05_OGW-SP experiment, while the observed N_i values fluctuate between these two simulations (Fig. 10a). The K22_OGW-SP experiment shows better agreement with observations at specific temperature levels (T ~ 210 K, ~220 K, and >230 K), while the LP05_OGW-SP experiment performs better at T~215K and ~225K. ~~The K22 scheme shows good agreement with observations for these cirrus clouds and the LP05 scheme produces reasonable results within or near the observed range.~~ The positive OGW-induced ΔN_i values in both schemes suggest that OGW-induced ice crystals are the dominant contributors to N_i ~~in~~during these 16 days ~~of cirrus~~

Formatted: Font: Italic

Formatted: Font: Italic

clouds (Fig. 10b). This indicates that ourThese findings demonstrate that our method is effective and provides a reliable method to distinguish orographic cirrus in flight campaigns.

However, the simulated N_i in the LP05_OGW-SP experiment for 16-day orographic cirrus is underestimated compared to the observations. This discrepancy is largely attributed to the inappropriate size settings for detrained ice crystals, which lead to a higher number of simulated detrained ice crystals over these 16 days. As we discussed in Section 4.2, the stronger competition in the LP05 scheme causes the simulated microphysical properties of cirrus clouds to be more sensitive to biases in other ice sources. Correcting these biases in the simulation would resolve the underestimations of N_i in the LP05 scheme.A comparison between results using a 20 μm size cut (Figs. 5, 6 and 10) and those using a 10 μm size cut (Figs. S18, S22 and S23) reveals that the observed N_i values decrease significantly when transitioning from the 10 μm to the 20 μm threshold. This reduction is because the concentration of ice crystals in the first size bin (5 – 15 μm) is significantly higher than those in subsequent larger bins, often dominating the total ice concentration (Jensen et al., 2013; Mitchell et al., 2024). Despite this decrease, OGW-induced ice crystals consistently remain the dominant contributor to total N_i. This consistency suggests that key signatures of homogeneous freezing are preserved across the two size thresholds, reinforcing robustness of our approach for identifying orographic cirrus clouds. Previous studies have highlighted that N_i in the first size bin (5 – 15 μm) measured by 2D-S probes may overestimate ice number concentrations (Jensen et al., 2013; Mitchell et al., 2024). Interestingly, the K22_OGW-SP experiment aligns closely with the observed N_i using the 10 μm size cut (Figs. S18, S22 and S23), potentially suggesting an overestimation of N_i in the K22 scheme. However, this interpretation remains uncertain without more reliable measurements on small ice crystals.

5. Summary and Conclusions

This study compares the newly introduced K22 ice nucleation scheme with the default LP05 ice nucleation scheme in the NCAR CAM6 model. The K22 scheme accounts for homogeneous nucleation, heterogeneous nucleation, their interactions, and competition with pre-existing ice. To investigate sources of ice crystals in cirrus clouds, we conduct 6six-year climatology simulations, considering with a focus on the effects of OGWs on ice nucleation. Additionally, nudged

experiments are performed for the SPARTICUS and ORCAS flight campaigns to further compares the two ice nucleation schemes. In all simulations, coarse mode dust is considered as the sole INPs.

In the six~~6~~-year climatology experiments, the K22_OGW-Climo experiment shows an increase in grid-mean N_i compared to the LP05_OGW-Climo experiment. Ice crystals detrained from convection are concentrated in low and mid-latitudes, while those formed due to OGWs are concentrated in mid- and high latitudes. Ice crystals due to turbulence are concentrated in low and mid-latitudes. Notably, homogeneous nucleation plays an important role in the global contribution to the total number of nucleated ice crystals.

The increase in ~~homogeneously~~ nucleated ice numbers in the K22 scheme compared to the LP05 scheme can be attributed to both direct and indirect reasons. The direct reason ~~relates to differences~~lies in their different assumptions of treating the ~~in the~~ competition ~~parameterization~~ between pre-existing ice~~the K22~~ and ~~LP05 schemes~~nucleated ice crystals. ~~To calculate the number of homogeneously nucleated ice crystals, the K22 scheme uses quenching speeds derived from the reduction of supersaturation caused by pre-existing ice crystals.~~The K22 scheme emphasizes the dynamic interplay between supersaturation, aerosol concentrations and pre-existing ice, allowing homogeneous nucleation, heterogeneous nucleation and the growth of pre-existing ice crystals to occur simultaneously. In contrast, the LP05 scheme is based on an empirical framework that favors a specific nucleation pathway. In the LP05 scheme, heterogeneous nucleation is favored at low supersaturation and high INP concentrations, while homogeneous nucleation dominates at high supersaturations. Pre-existing ice crystals consume supersaturation before new ice nucleation can occur. ~~compares the number of pre-existing ice crystals to the theoretical number of homogeneously nucleated ice crystals in the absence of pre-existing ice.~~ This may result~~s~~ in a stronger ~~more frequent~~ competition in the LP05 scheme, suppressing homogeneous nucleation.

The indirect reason ~~arises from~~is related to the increase in ice number concentrations within the K22 scheme, which appears to lead~~s~~ to higher cloud frequency. This ~~is~~ can be ~~because~~ due to the presence of smaller ice crystals in the K22 scheme, which have lower fall speeds ~~have longer lifetimes~~, allowing them to travel over broader regions before completely sublimated. ~~Changes~~ An increase in cloud frequency may induce changes in global temperature, ~~which in turn~~ potentially affecting turbulence and ~~global circulation. Altered circulation dynamics influence the~~ subgrid-scale vertical velocity

~~variance associated with ice nucleation~~, thereby impacting ice ~~formation~~nucleation. However, these factors are not the key factors that cause the significant increase in N_i.

In addition, the global increase in coarse mode dust concentrations leads to a higher number of heterogeneously nucleated ice crystals. However, i~~I~~mproved aerosol wet removal parameterization due to convection can mitigate this effect by reducing the concentration of coarse mode dust in the upper troposphere.

The nudged experiments conducted during the SPARTICUS flight campaign specifically focus on orographic cirrus clouds. The K22_OGW-SP experiment generates microphysical properties comparable to those of the LP05_OGW-SP experiment, with both aligning ~~well~~reasonable with observational data. However, the K22_OGW-SP experiment~~it~~ tends to produce a higher number of smaller ice crystals compared to the LP05_OGW-SP experiment. Both the LP05 and K22 schemes identify OGWs as the dominant ice crystal source in orographic cirrus clouds observed during SPARTICUS, but the LP05 scheme exhibits greater competition from detrainment and turbulence sources than the K22 scheme. In addition, the K22_OGW-SP experiment simulates homogeneous nucleation as the dominant mechanism in orographic cirrus formation.

The ORCAS flight campaign is used to further evaluate the simulation results for both the K22 and LP05 schemes. Due to instrument limitations in measuring ice crystals, 2D-C probes are utilized during the ORCAS campaign, ~~allowing for~~providing reliable observations of ~~large-size ice crystal~~ the microphysical properties of large-size ice crystal ($D_{num} \geq$ 62.5μm). To better evaluate the results, the flight data is divided into three regions~~. are divided.~~ Region 1 encompasses flights over high mountains, while Regions 2 and 3 cover flights mostly over oceans~~, greatly influenced by moist conditions~~. Region 2, located downwind of the Andes Mountains and high plateaus in Antarctic, is also affected by orographic cirrus clouds, which impact the observed cloud microphysical properties.

~~The overall microphysical properties in these three regions are not well represented in the OGW experiments for both the K22 and LP05 schemes compared to observations. This discrepancy arises because the model struggles to simulate the dominant ice sources over oceanic regions. It underscores the importance of incorporating the dominant ice sources into the model to effectively reproduce the observed characteristics of cirrus clouds.~~

Formatted: Font: Italic

Formatted: Subscript

~~The differences in moisture availability and dynamic environmental conditions between land and ocean result in distinct cloud microphysical behaviours and ice nucleation processes, resulting in unique characteristics of cirrus clouds in these two environments.~~

~~Over land, particularly in mountainous regions, the air is relatively dry, leading to low observed and simulated IWC. However, the high vertical velocities provided by mountains foster favourable conditions for homogeneous nucleation, which often becomes the dominant nucleation mechanism in orographic cirrus clouds. These clouds can exhibit high ice number concentrations and reach very high altitudes. Consequently, incorporating OGWs in ice nucleation processes allows the model to better simulate cirrus clouds over land.~~

~~In contrast, over oceans, the atmosphere is rich in water vapor, resulting in high observed IWC. However, the lack of vertical velocity sources in the upper troposphere over oceans results in heterogeneous nucleation being the dominant mechanism. Ice crystals due to gravity waves, such as frontal and convective gravity waves, can be important ice sources in these regions. In addition, some critical INPs are absent in current ice nucleation schemes. As a result, the model performs poorly in simulating cirrus clouds over oceans. To address the absence of crucial ice sources in these simulations, further studies should incorporate additional dynamic factors, such as frontal gravity waves and convective gravity waves, as well as other types of INPs.~~

~~In conclusion, an accurate representation of the competition mechanism in the ice nucleation scheme is crucial, particularly for the interactions between pre-existing and newly nucleated ice crystals, as these interactions can significantly influence the simulated microphysical properties of cirrus clouds. While many studies primarily focus on the dominant ice sources, minor sources are often overlooked. However, our studies suggest that minor ice sources may also influence cloud microphysical properties through competition mechanisms between pre-existing and newly nucleated ice crystals. Understanding these dynamics is essential for accurately simulating the behaviours and characteristics of cirrus clouds under different atmospheric conditions.~~

Moreover, distinguishing ice crystal sources has long posed a significant challenge in the study of cirrus clouds. The different behaviours between dominant and minor ice sources ~~in high N_i regions~~ with the K22 and LP05 schemes provide a reasonable method for ~~distinguishing~~ identifying cirrus cloud types in observations, ~~especially for~~particularly orographic

cirrus. ~~By a~~Applying this method to ~~categorize orographic cirrus in~~ the SPARTICUS campaign, we identify 16 flight days ~~of flight~~ during which OGW-induced ice source dominates the ice formation, with no significant ~~underestimation~~bias of N_i in either scheme. These selected~~identified~~ flights exhibit reasonable~~a good~~ agreement in microphysical properties with observations, proving that this method is effective for distinguishing orographic cirrus from observations.

Furthermore, our comparison between~~of~~ simulated cirrus clouds with observations highlights the need for refining the model representation of key processes governing cirrus cloud evolution.~~,~~ They includ~~cing detrainment,~~ ice crystal growth (ice deposition and accretion), secondary ice production, sublimation, and ice crystal sedimentation. Differences in moisture availability and dynamic conditions between land and ocean also may lead to distinct cloud microphysical behaviors, resulting in unique cirrus cloud characteristics across these regions. Over land, particularly in mountainous regions, strong vertical velocities induced by mountains create favourable conditions for homogeneous ice nucleation, which often becomes the dominant nucleation mechanism in orographic cirrus clouds. In contrast, over oceans, the scarcity of strong vertical velocity sources in the upper troposphere over oceans results in heterogeneous nucleation being the prevailing nucleation mechanism. We note~~(Yook et al., 2025)~~ that other critical INPs (such as black carbon, metallic particles, biological materials) besides mineral dust are not currently represented in ice nucleation schemes (Lin et al., 2025). Further studies should also consider incorporating additional dynamic processes, such as frontal and convective gravity waves (Yook et al., 2025). In addition to gravity waves, uncertainties in the representation of other drivers of ice sources, such as turbulence and convective detrainment, should be reduced. Recent incorporations of convective cloud microphysics in deep convection (Lin et al., 2021; Song & Zhang, 2011) should help to reduce the uncertainty in detrained ice properties. Further evaluations of the K22 scheme based on model climatology will be conducted by comparing modelled cirrus with regional observational datasets (Krämer et al., 2016; Krämer et al., 2020) and global satellite data (Lyu et al., 2023).

~~Over land, particularly in mountainous regions, the air is relatively dry, leading to low observed and simulated IWC. However, the high vertical velocities provided by mountains foster favourable conditions for homogeneous nucleation, which often becomes the dominant nucleation mechanism in orographic cirrus clouds. These clouds can exhibit high ice~~

~~number concentrations and reach very high altitudes. Consequently, incorporating OGWs in ice nucleation processes allows the model to better simulate cirrus clouds over land.~~

Code and data availability. For readers interested in replicating specific aspects of our study, we encourage them to contact the corresponding authors of the cited papers for access to the underlying code and data.

Author contributions. KL: incorporated K22 scheme into CAM6, conducted simulations, analyzed results, wrote the article; XL: provided guidance, reviewed the manuscript; BK: provided K22 nucleation parameterization and reviewed the manuscript.

Competing interests. At least one of the (co-)authors is a member of the editorial board of Atmospheric Chemistry of Physics.

Disclaimer. Publisher's note: Copernicus Publications remains neutral with regard to jurisdictional claims made in the text, published maps, institutional affiliations, or any other geographical representation in this paper. While Copernicus Publications makes every effort to include appropriate place names, the final responsibility lies with the authors.

Acknowledgement. This work was supported by the National Aeronautics and Space Administration (NASA) grant (No. ROSES-2020 80NSSC21K1457).

Financial support. This research has been supported by the National Aeronautics and Space Administration (NASA) grant (No. ROSES-2020 80NSSC21K1457).

References

Baumgartner, M., Rolf, C., Grooß, J. U., Schneider, J., Schorr, T., Möhler, O., Spichtinger, P., & Krämer, M. (2022). New investigations on homogeneous ice nucleation: the effects of water activity and water saturation formulations. *Atmos. Chem. Phys.*, *22*(1), 65-91. https://doi.org/10.5194/acp-22-65-2022

Beall, C. M., Hill, T. C. J., DeMott, P. J., Köneman, T., Pikridas, M., Drewnick, F., Harder, H., Pöhlker, C., Lelieveld, J., Weber, B., Iakovides, M., Prokeš, R., Sciare, J., Andreae, M. O., Stokes, M. D., & Prather, K. A. (2022). Ice-nucleating particles near two major dust source regions. *Atmos. Chem. Phys.*, *22*(18), 12607-12627. https://doi.org/10.5194/acp-22-12607-2022

Bogenschutz, P. A., Gettelman, A., Morrison, H., Larson, V. E., Craig, C., & Schanen, D. P. (2013). Higher-Order Turbulence Closure and Its Impact on Climate Simulations in the Community Atmosphere Model. *Journal of Climate*, *26*(23), 9655-9676 , ISSN = 0894-8755 , DOI = https //doi.org/9610.1175/jcli-d-9613-00075.00071. https://journals.ametsoc.org/view/journals/clim/26/23/jcli-d-13-00075.1.xml

Boucher, O., Randall, D., Artaxo, P., Bretherton, C., Feingold, G., Forster, P., Kerminen, V.-M., Kondo, Y., Liao, H., Lohmann, U., Rasch, P., Satheesh, S., Sherwood, S., Stevens, B., & Zhang, X. (2013). Clouds and Aerosols. In (pp. 571-892).

Chen, J., Wu, Z., Gong, X., Qiu, Y., Chen, S., Zeng, L., & Hu, M. (2024). Anthropogenic Dust as a Significant Source of Ice-Nucleating Particles in the Urban Environment. *Earth's Future*, *12*(1), e2023EF003738. https://doi.org/https://doi.org/10.1029/2023EF003738

Danabasoglu, G., Lamarque, J. F., Bacmeister, J., Bailey, D. A., DuVivier, A. K., Edwards, J., Emmons, L. K., Fasullo, J., Garcia, R., Gettelman, A., Hannay, C., Holland, M. M., Large, W. G., Lauritzen, P. H., Lawrence, D. M., Lenaerts, J. T. M., Lindsay, K., Lipscomb, W. H., Mills, M. J., . . . Strand, W. G. (2020). The Community Earth System Model Version 2 (CESM2). *Journal of Advances in Modeling Earth Systems*, *12*(2), e2019MS001916. https://agupubs.onlinelibrary.wiley.com/doi/abs/10.1029/2019MS001916

Eidhammer, T., Morrison, H., Bansemer, A., Gettelman, A., & Heymsfield, A. (2014). Comparison of ice cloud properties simulated by the Community Atmosphere Model (CAM5) with in-situ observations. *Atmospheric Chemistry & Physics*, *14*(18). https://doi.org/https://doi.org/10.5194/acp-14-10103-2014

Fan, J., Wang, Y., Rosenfeld, D., & Liu, X. (2016). Review of Aerosol-Cloud Interactions: Mechanisms, Significance and Challenges. *Journal of the Atmospheric Sciences*, *73*. https://doi.org/10.1175/JAS-D-16-0037.1

Forster, P., Storelvmo, T., Armour, K., Collins, W., Dufresne, J.-L., Frame, D., Lunt, D. J., Mauritsen, T., Palmer, M. D., Watanabe, M., Wild, M., & Zhang, H. (2023). The Earth's Energy Budget, Climate Feedbacks and Climate Sensitivity. In (pp. 923-1054). https://doi.org/10.1017/9781009157896.009

Froyd, K. D., Yu, P., Schill, G. P., Brock, C. A., Kupc, A., Williamson, C. J., Jensen, E. J., Ray, E., Rosenlof, K. H., Bian, H., Darmenov, A. S., Colarco, P. R., Diskin, G. S., Bui, T., & Murphy, D. M. (2022). Dominant role of mineral dust in cirrus cloud formation revealed by global-scale measurements. *Nature Geoscience*, *15*(3), 177-183. https://doi.org/10.1038/s41561-022-00901-w

Gasparini, B., Sullivan, S. C., Sokol, A. B., Kärcher, B., Jensen, E., & Hartmann, D. L. (2023). Opinion: Tropical cirrus – from micro-scale processes to climate-scale impacts. *Atmos. Chem. Phys.*, *23*(24), 15413-15444. https://doi.org/10.5194/acp-23-15413-2023

Gettelman, A., Liu, X., Ghan, S. J., Morrison, H., Park, S., Conley, A. J., Klein, S. A., Boyle, J., Mitchell, D. L., & Li, J.-L. F. (2010). Global simulations of ice nucleation and ice supersaturation with an improved cloud scheme in the Community Atmosphere Model. *Journal of Geophysical Research: Atmospheres*, *115*(D18). https://doi.org/https://doi.org/10.1029/2009JD013797

Gettelman, A., & Morrison, H. (2015). Advanced Two-Moment Bulk Microphysics for Global Models. Part I: Off-Line Tests and Comparison with Other Schemes. *Journal of Climate*, *28*(3), 1268-1287 , ISSN = 0894-8755 , DOI = https //doi.org/1210.1175/jcli-d-1214-00102.00101. https://journals.ametsoc.org/view/journals/clim/28/3/jcli-d-14-00102.1.xml

Glienke, S., & Mei, F. (2019). *Two-Dimensional Stereo (2D-S) Probe Instrument Handbook*. https://www.osti.gov/biblio/1597436 https://www.osti.gov/servlets/purl/1597436

Golaz, J.-C., Larson, V. E., & Cotton, W. R. (2002a). A PDF-Based Model for Boundary Layer Clouds. Part I: Method and Model Description. *Journal of the Atmospheric Sciences*, *59*(24), 3540-3551 , ISSN = 0022-4928 , DOI = https //doi.org/3510.1175/1520-0469. https://journals.ametsoc.org/view/journals/atsc/59/24/1520-0469_2002_059_3540_apbmfb_2.0.co_2.xml

Golaz, J.-C., Larson, V. E., & Cotton, W. R. (2002b). A PDF-Based Model for Boundary Layer Clouds. Part II: Model Results. *Journal of the Atmospheric Sciences*, *59*(24), 3552-3571 , ISSN = 0022-4928 , DOI = https //doi.org/3510.1175/1520-0469. https://journals.ametsoc.org/view/journals/atsc/59/24/1520-0469_2002_059_3552_apbmfb_2.0.co_2.xml

Heymsfield, A. J., Krämer, M., Luebke, A., Brown, P., Cziczo, D. J., Franklin, C., Lawson, P., Lohmann, U., McFarquhar, G., Ulanowski, Z., & Van Tricht, K. (2017). Cirrus Clouds. *Meteorological Monographs*, *58*, 2.1-2.26. https://doi.org/https://doi.org/10.1175/AMSMONOGRAPHS-D-16-0010.1

Hinz, K.-P., Kaufmann, R., & Spengler, B. (1996). Simultaneous Detection of Positive and Negative Ions From Single Airborne Particles by Real-time Laser Mass Spectrometry. *Aerosol Science and Technology*, *24*(4), 233-242. https://doi.org/10.1080/02786829608965368

Horner, G., & Gryspeerdt, E. (2023). The evolution of deep convective systems and their associated cirrus outflows. *Atmos. Chem. Phys.*, *23*(22), 14239-14253. https://doi.org/10.5194/acp-23-14239-2023

Horner, G., & Gryspeerdt, E. (2024, April 01, 2024). *How does the lifetime of cirrus detrained from deep convection impact the cloud radiative effect of the tropics?* EGU General Assembly Conference Abstracts, Vienna, Austria. https://ui.adsabs.harvard.edu/abs/2024EGUGA..2613338H

Huang, M., Xiao, H., Wang, M., & Fast, J. D. (2020). Assessing CLUBB PDF Closure Assumptions for a Continental Shallow-to-Deep Convective Transition Case Over Multiple Spatial Scales. *Journal of Advances in Modeling Earth Systems*, *12*(10), e2020MS002145. https://doi.org/https://doi.org/10.1029/2020MS002145

Iacono, M. J., Delamere, J. S., Mlawer, E. J., Shephard, M. W., Clough, S. A., & Collins, W. D. (2008). Radiative forcing by long-lived greenhouse gases: Calculations with the AER radiative transfer models. *Journal of Geophysical Research: Atmospheres*, *113*(D13). https://agupubs.onlinelibrary.wiley.com/doi/abs/10.1029/2008JD009944

Jensen, E. J., Lawson, R. P., Bergman, J. W., Pfister, L., Bui, T. P., & Schmitt, C. G. (2013). Physical processes controlling ice concentrations in synoptically forced, midlatitude cirrus. *Journal of Geophysical Research: Atmospheres*, *118*(11), 5348-5360. https://doi.org/https://doi.org/10.1002/jgrd.50421

Kärcher, B. (2022). A Parameterization of Cirrus Cloud Formation: Revisiting Competing Ice Nucleation. *Journal of Geophysical Research: Atmospheres*, *127*(18), e2022JD036907. https://doi.org/https://doi.org/10.1029/2022JD036907

Kärcher, B., DeMott, P. J., Jensen, E. J., & Harrington, J. Y. (2022). Studies on the Competition Between Homogeneous and Heterogeneous Ice Nucleation in Cirrus Formation. *Journal of Geophysical Research: Atmospheres*, *127*(3), e2021JD035805. https://doi.org/https://doi.org/10.1029/2021JD035805

Kärcher, B., Hendricks, J., & Lohmann, U. (2006). Physically based parameterization of cirrus cloud formation for use in global atmospheric models. *Journal of Geophysical Research: Atmospheres*, *111*(D1). https://doi.org/https://doi.org/10.1029/2005JD006219

Kärcher, B., & Podglajen, A. (2019). A Stochastic Representation of Temperature Fluctuations Induced by Mesoscale Gravity Waves. *Journal of Geophysical Research: Atmospheres*, *124*(21), 11506-11529. https://agupubs.onlinelibrary.wiley.com/doi/abs/10.1029/2019JD030680

Kärcher, B., & Ström, J. (2003). The roles of dynamical variability and aerosols in cirrus cloud formation. *Atmos. Chem. Phys.*, *3*(3), 823-838. https://acp.copernicus.org/articles/3/823/2003/

Knopf, D. A., & Alpert, P. A. (2023). Atmospheric ice nucleation. *Nature Reviews Physics*, *5*(4), 203-217. https://doi.org/10.1038/s42254-023-00570-7

Koop, T., Luo, B., Tsias, A., & Peter, T. (2000). Water activity as the determinant for homogeneous ice nucleation in aqueous solutions. *Nature*, *406*(6796), 611-614. https://doi.org/10.1038/35020537

Krämer, M., Rolf, C., Luebke, A., Afchine, A., Spelten, N., Costa, A., Meyer, J., Zöger, M., Smith, J., Herman, R. L., Buchholz, B., Ebert, V., Baumgardner, D., Borrmann, S., Klingebiel, M., & Avallone, L. (2016). A microphysics guide to cirrus clouds – Part 1: Cirrus types. *Atmos. Chem. Phys.*, *16*(5), 3463-3483. https://acp.copernicus.org/articles/16/3463/2016/

Krämer, M., Rolf, C., Spelten, N., Afchine, A., Fahey, D., Jensen, E., Khaykin, S., Kuhn, T., Lawson, P., Lykov, A., Pan, L. L., Riese, M., Rollins, A., Stroh, F., Thornberry, T., Wolf, V., Woods, S., Spichtinger, P., Quaas, J., & Sourdeval, O. (2020). A microphysics guide to cirrus – Part 2: Climatologies of clouds and humidity from observations. *Atmos. Chem. Phys.*, *20*(21), 12569-12608. https://acp.copernicus.org/articles/20/12569/2020/

Lawson, R. P. (2011). Effects of ice particles shattering on the 2D-S probe. *Atmos. Meas. Tech.*, *4*(7), 1361-1381. https://doi.org/https://doi.org/10.5194/amt-4-1361-2011

Lin, L., Fu, Q., Liu, X., Shan, Y., Giangrande, S. E., Elsaesser, G. S., Yang, K., & Wang, D. (2021). Improved Convective Ice Microphysics Parameterization in the NCAR CAM Model. *Journal of Geophysical Research: Atmospheres*, *126*(9), e2020JD034157. https://doi.org/https://doi.org/10.1029/2020JD034157

Lin, L., Liu, X., Zhao, X., Shan, Y., Ke, Z., Lyu, K., & Bowman, K. P. (2025). Ice nucleation by volcanic ash greatly alters cirrus cloud properties. *Science Advances*, *11*(19), eads0572. https://doi.org/doi:10.1126/sciadv.ads0572

Liou, K.-N. (1986). Influence of Cirrus Clouds on Weather and Climate Processes: A Global Perspective. *Monthly Weather Review*, *114*(6), 1167-1199. https://doi.org/10.1175/1520-0493(1986)114<1167:Ioccow>2.0.Co;2

Liu, X., Ma, P. L., Wang, H., Tilmes, S., Singh, B., Easter, R. C., Ghan, S. J., & Rasch, P. J. (2016). Description and evaluation of a new four-mode version of the Modal Aerosol Module (MAM4) within version 5.3 of the Community Atmosphere Model. *Geosci. Model Dev.*, *9*(2), 505-522. https://gmd.copernicus.org/articles/9/505/2016/

Liu, X., & Penner, J. (2005). Ice nucleation parameterization for global models. *Meteorologische Zeitschrift*, *14*, 499-514 , DOI = https //doi.org/410.1127/0941-2948/2005/0059.

Liu, X., Penner, J. E., Ghan, S. J., & Wang, M. (2007). Inclusion of ice microphysics in the NCAR Community Atmospheric Model version 3 (CAM3). *Journal of Climate*, *20*(18), 4526-4547 , ISSN = 1520-0442 , DOI = https //doi.org/4510.1175/JCLI4264.4521.

Lyu, K., Liu, X., Bacmeister, J., Zhao, X., Lin, L., Shi, Y., & Sourdeval, O. (2023). Orographic Cirrus and Its Radiative Forcing in NCAR CAM6. *Journal of Geophysical Research: Atmospheres*, *128*(10), e2022JD038164. https://agupubs.onlinelibrary.wiley.com/doi/abs/10.1029/2022JD038164

Mitchell, D. L., Garnier, A. E., & Woods, S. (2024). Advances in CALIPSO (IIR) cirrus cloud property retrievals – Part 1: Methods and testing. *EGUsphere*, *2024*, 1-44. https://doi.org/10.5194/egusphere-2024-3790

Morrison, H., & Gettelman, A. (2008). A New Two-Moment Bulk Stratiform Cloud Microphysics Scheme in the Community Atmosphere Model, Version 3 (CAM3). Part I: Description and Numerical Tests. *Journal of Climate*, *21*(15), 3642-3659 , ISSN = 0894-8755 , DOI = 3610.1175/2008jcli2105.3641. https://journals.ametsoc.org/view/journals/clim/21/15/2008jcli2105.1.xml

Muhlbauer, A., Ackerman, T. P., Comstock, J. M., Diskin, G. S., Evans, S. M., Lawson, R. P., & Marchand, R. T. (2014). Impact of large-scale dynamics on the microphysical properties of midlatitude cirrus. *Journal of Geophysical Research: Atmospheres*, *119*(7), 3976-3996. https://agupubs.onlinelibrary.wiley.com/doi/abs/10.1002/2013JD020035

Muhlbauer, A., Kalesse, H., & Kollias, P. (2014). Vertical velocities and turbulence in midlatitude anvil cirrus: A comparison between in situ aircraft measurements and ground-based Doppler cloud radar retrievals. *Geophysical Research Letters*, *41*(22), 7814-7821. https://agupubs.onlinelibrary.wiley.com/doi/abs/10.1002/2014GL062279

Muri, H., Kristjánsson, J. E., Storelvmo, T., & Pfeffer, M. A. (2014). The climatic effects of modifying cirrus clouds in a climate engineering framework. *Journal of Geophysical Research: Atmospheres*, *119*(7), 4174-4191. https://doi.org/https://doi.org/10.1002/2013JD021063

Murray, B. J., & Liu, X. (2022). Chapter 15 - Ice-nucleating particles and their effects on clouds and radiation. In K. S. Carslaw (Ed.), *Aerosols and Climate* (pp. 619-649). Elsevier. https://doi.org/https://doi.org/10.1016/B978-0-12-819766-0.00014-6

Nugent, J. M., Turbeville, S. M., Bretherton, C. S., Blossey, P. N., & Ackerman, T. P. (2022). Tropical Cirrus in Global Storm-Resolving Models: 1. Role of Deep Convection. *Earth and Space Science*, *9*(2), e2021EA001965. https://doi.org/https://doi.org/10.1029/2021EA001965

Patnaude, R., Diao, M., Liu, X., & Chu, S. (2021). Effects of thermodynamics, dynamics and aerosols on cirrus clouds based on in situ observations and NCAR CAM6. *Atmos. Chem. Phys.*, *21*(3), 1835-1859. https://acp.copernicus.org/articles/21/1835/2021/

Pruppacher, H. R., Klett, J. D., & Wang, P. K. (1998). Microphysics of clouds and precipitation. In: Taylor & Francis.

Sassen, K., & Cho, B. S. (1992). Subvisual-Thin Cirrus Lidar Dataset for Satellite Verification and Climatological Research. *Journal of Applied Meteorology and Climatology*, *31*(11), 1275-1285. https://doi.org/https://doi.org/10.1175/1520-0450(1992)031<1275:STCLDF>2.0.CO;2

Sassen, K., Wang, Z., & Liu, D. (2008). Global distribution of cirrus clouds from CloudSat/Cloud-Aerosol Lidar and Infrared Pathfinder Satellite Observations (CALIPSO) measurements. *Journal of Geophysical Research: Atmospheres*, *113*(D8). https://doi.org/https://doi.org/10.1029/2008JD009972

Shan, Y., Liu, X., Lin, L., Ke, Z., & Lu, Z. (2021). An Improved Representation of Aerosol Wet Removal by Deep Convection and Impacts on Simulated Aerosol Vertical Profiles. *Journal of Geophysical Research: Atmospheres*, *126*(13), e2020JD034173. https://agupubs.onlinelibrary.wiley.com/doi/abs/10.1029/2020JD034173

Shi, X., Liu, X., & Zhang, K. (2015). Effects of pre-existing ice crystals on cirrus clouds and comparison between different ice nucleation parameterizations with the Community Atmosphere Model (CAM5). *Atmos. Chem. Phys.*, *15*(3), 1503-1520. https://acp.copernicus.org/articles/15/1503/2015/

Song, X., & Zhang, G. J. (2011). Microphysics parameterization for convective clouds in a global climate model: Description and single-column model tests. *Journal of Geophysical Research: Atmospheres*, *116*(D2). https://doi.org/https://doi.org/10.1029/2010JD014833

Spang, R., Müller, R., & Rap, A. (2024). Radiative effect of thin cirrus clouds in the extratropical lowermost stratosphere and tropopause region. *Atmos. Chem. Phys.*, *24*(2), 1213-1230. https://doi.org/10.5194/acp-24-1213-2024

Stephens, B. B., Long, M. C., Keeling, R. F., Kort, E. A., Sweeney, C., Apel, E. C., Atlas, E. L., Beaton, S., Bent, J. D., Blake, N. J., Bresch, J. F., Casey, J., Daube, B. C., Diao, M., Diaz, E., Dierssen, H., Donets, V., Gao, B.-C., Gierach, M., . . . Watt, A. S. (2018). The O2/N2 Ratio and CO2 Airborne Southern Ocean Study. *Bulletin of the American Meteorological Society*, *99*(2), 381-402. https://doi.org/https://doi.org/10.1175/BAMS-D-16-0206.1

Tobo, Y., Adachi, K., DeMott, P., Hill, T., Hamilton, D., Mahowald, N., Nagatsuka, N., Ohata, S., Uetake, J., Kondo, Y., & Koike, M. (2019). Glacially sourced dust as a potentially significant source of ice nucleating particles. *Nature Geoscience*, *12*, 1-6. https://doi.org/10.1038/s41561-019-0314-x

Wang, P.-H., Minnis, P., McCormick, M. P., Kent, G. S., & Skeens, K. M. (1996). A 6-year climatology of cloud occurrence frequency from Stratospheric Aerosol and Gas Experiment II observations (1985–1990). *Journal of Geophysical Research: Atmospheres*, *101*(D23), 29407-29429. https://doi.org/https://doi.org/10.1029/96JD01780

Winker, D. M. P. J. C. J. A. A. S. A. C. R. J. C. P. R. F. P. F. Q. H. R. M., & Wielicki, B. A. (2010). The CALIPSO mission. *Bulletin of the American Meteorological Society*, *91(9), 1211–1230. , DOI = https://doi.org/10.1175/2010BAMS3009.1*.

Yook, S., Solomon, S., Weimer, M., Kinnison, D., Garcia, R., & Stone, K. (2025). Implementation of Sub-Grid Scale Temperature Perturbations Induced by Non-Orographic Gravity Waves in WACCM6. *Journal of Advances in Modeling Earth Systems*, *17*. https://doi.org/10.1029/2024MS004625

Zhang, G. J., & McFarlane, N. A. (1995). Sensitivity of climate simulations to the parameterization of cumulus convection in the Canadian climate centre general circulation model. *Atmosphere-Ocean*, *33*(3), 407-446. https://doi.org/10.1080/07055900.1995.9649539